# Collapse of the clock tower in Finale Emilia after the May 2012 Emilia Romagna earthquake sequence: Numerical insight

Maurizio Acito, Massimiliano Bocciarelli, Claudio Chesi, Gabriele Milani *

*Department of Architecture, Built Environment and Construction Engineering ABC, Politecnico di Milano, Piazza Leonardo da Vinci 32, 20133 Milan, Italy*

*Article history:*
Received 26 December 2013
Revised 10 April 2014
Accepted 10 April 2014
Available online 9 May 2014

## 1. Introduction

A cooperation agreement between the Italian Ministry for the architectural heritage (MiBAC) and the Technical University of Milan, with scientific responsibility by the authors, has allowed carrying out wide and comprehensive numerical analyses [1,2] aimed at better understanding the causes of the collapse, occurred during the May 2012 seismic events and subsequent aftershocks, of two meaningful monuments in Finale Emilia (Italy).

The primary effort is to provide detailed information for the reconstruction, after the clear identification of the structural causes at the base of the collapses observed.

The two monuments under study are the ancient town clock tower and the castle; this last is the object of a detailed structural analysis still under study [1].

* Corresponding author. Tel.: +39 022399 4290; fax: +39 022399 4220.
*E-mail address:* gabriele.milani@polimi.it (G. Milani).

The clock tower became the symbol of the earthquake and many images of its precarious equilibrium conditions after the main shock are available on the net, showing one half of the structure still uncollapsed near the other collapsed into ruins, see Fig. 1, with a vertical crack passing roughly through the middle of the clock.

At present, there is a wide literature available dealing with the static and seismic analysis of masonry towers [3–18], ranging from experimental works [3–7], dynamic identification [8,9], and complex non-linear static (pushover) and dynamic analyses [10–18]. Pushover comprises both standard [14,18] and multi-modal approaches [17], which appear more suited for slender structures. Usually, Finite Elements FEs are required to have a realistic insight into the reasons of structural weakness and seismic vulnerability of each specific case, and even within the FE framework, different levels of complexity exist, both for what concerns the geometric discretization (from 1D [11,12] to 3D models [13–15], passing through plate and shell approaches [16]), the typology of analyses

**Fig. 1.** Meaningful images of the survived part of the tower after the 20th May seismic event.

performed (static, e.g. [14] or dynamic, e.g. [16]) and the material models adopted (e.g. simplified procedures with no tension material models [12], elasto-plastic or limit analysis approaches [14,18], models with damage [17,18], etc.).

In this framework, the present paper is aimed at using different numerical strategies, exhibiting increasing level of complexity and accuracy, for the post-earthquake structural analysis of a case study, which can be considered as paradigmatic of the actual behavior of historical masonry towers.

The tower (Figs. 2 and 3), now almost completely collapsed, was located in Finale Emilia, a small but strategically important town – in the Medieval age – near Ferrara, the ancient capital of the Estense Dukedom, on the Panaro river, not far from its confluence into the Po river. Finale was strategically very important for the Estense Dukedom because of the morphology of the country, which exhibited a clepsydra shape, with Finale Emilia and San Felice sul Panaro located in the middle of the clepsydra. From Finale, indeed, it was possible to control the passage of the goods transported through the river and at the same time strategically defend the Dukedom in case of war by the neighboring countries (Bologna and Mirandola).

The clock tower and the castle were located at the extremes of the walled city, in correspondence of the river. The control of the ships occurred therefore with a twofold check conducted in both directions, from the tower and the castle.

About one hundred years ago, the municipality decided for public health reasons to bury the portion of the river streaming within the walls and to deviate it outside Finale Emilia. A vintage photo taken at the beginning of the XX century shows the tower when the river was still present, see Fig. 4.

The tower had a slenderness – defined as the ratio between the overall height of the structure and the smallest dimension of the base cross section – roughly equal to 4. Therefore it typically suffered of reduced stability problems connected to second order effects coming from the vertical loads, due to possible tilting.

Only recently, the Italian building code [19–22] has changed the definition of the seismic zones, including parts of the territory which previously were not classified as seismic; this was the case of the portion of the Emilia-Romagna region stricken by the earthquake, where the structure was located.

Several numerical analyses have been conducted and are here discussed; most of them based on sophisticated approaches proposed in the technical literature, where the topic of ancient masonry towers has been largely investigated, as it is documented by the large number of works mentioned in the references. In this specific study, attention is focused on the interpretation of the collapse modalities induced by the seismic actions. The performed analyses have provided the opportunity to validate the computational model in the non-linear phase, i.e., through the reproduction of the non-linear response, whereas validation of models can be normally performed only in the linear field by means of a comparison with the structural frequencies and modes experimentally measured.

The performed analyses, aimed at investigating the seismic behavior of the structure, comprise (1) the evaluation of the vulnerability indices according to the Italian Guidelines on the

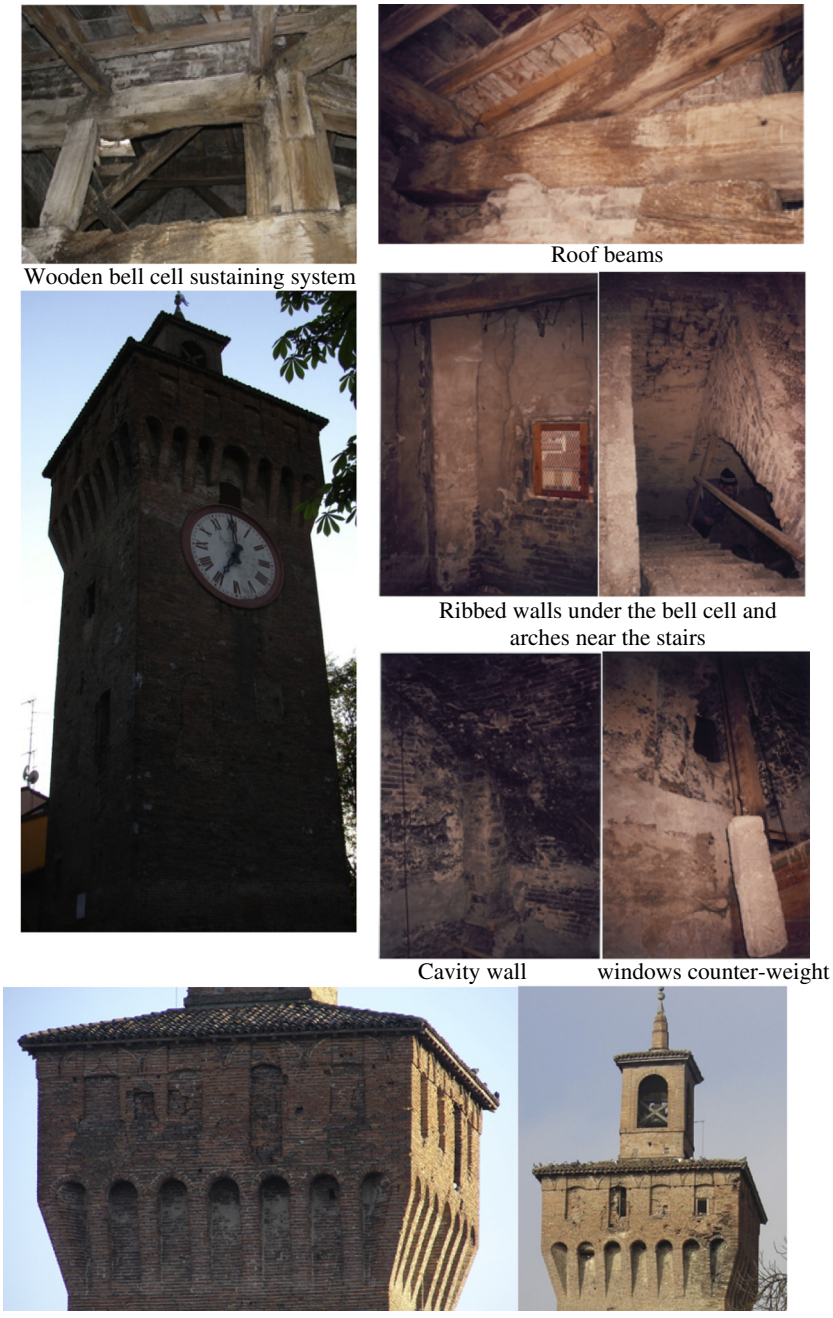


**Fig. 2.** The clock tower before the collapse. Pictures of the overall tower and details describing some interesting geometrical issues.

architectural heritage [23], by means of response spectrum and linear static analyses, the latter conducted with reference to both the design spectrum prescribed by the Italian code and spectra corresponding to real acceleration recordings taken during the seismic event; (2) N2 investigations, where the seismic demand in terms of the inelastic acceleration–displacement AD spectrum is compared with the 1 DOF equivalent response determined by means of non-linear three dimensional pushover analyses along the two inertia directions with two different distributions of the horizontal loads (G1 and G2 according to the Italian code) and (3) a full non-linear dynamic analysis with the input accelerogram registered during the 20th May seismic event taking into consideration both geometrical (large displacement effects) and material (elasto plastic damage behavior of the masonry) non-linearities. Additional full 3D limit analyses along x and y axis and G1 distributions are conducted with an ad-hoc software [24], where a Mohr–Coulomb failure criterion is adopted for masonry, to further assess collapse loads and failure mechanisms found with the pushover analyses.

Pushover analyses are conducted by means of Strand7 [25] commercial code, assuming that masonry behaves as an elastic-perfectly plastic material obeying a Mohr–Coulomb failure criterion.

Finally, 3D non-linear dynamic analyses, based on an isotropic damage model have been performed under ABAQUS [26] environment. As a matter of fact, non-linear dynamic analysis methods for masonry structures require further research efforts before they can be confidently used in standard design, but for sure they represent the most reliable method to determine the seismic vulnerability of such structures for their capacity to take into account also the effect of the higher modes.

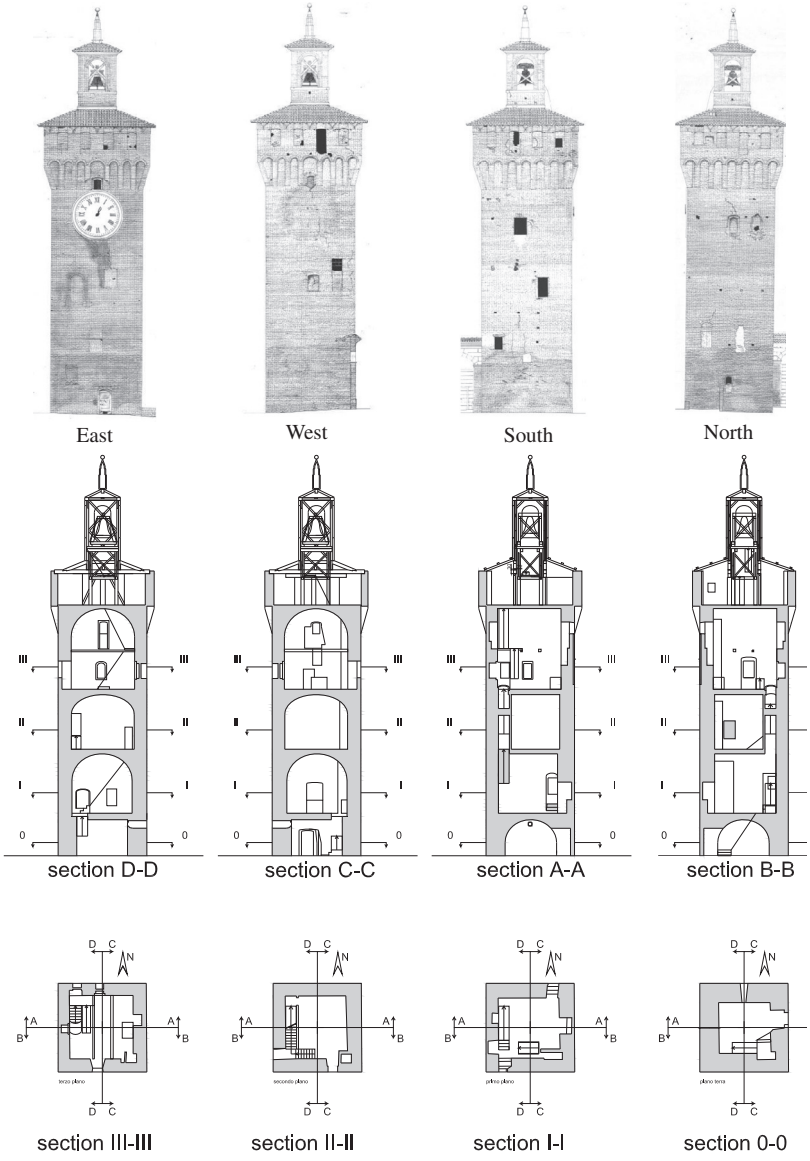


**Fig. 3.** Lateral views, vertical and horizontal sections of the clock tower.

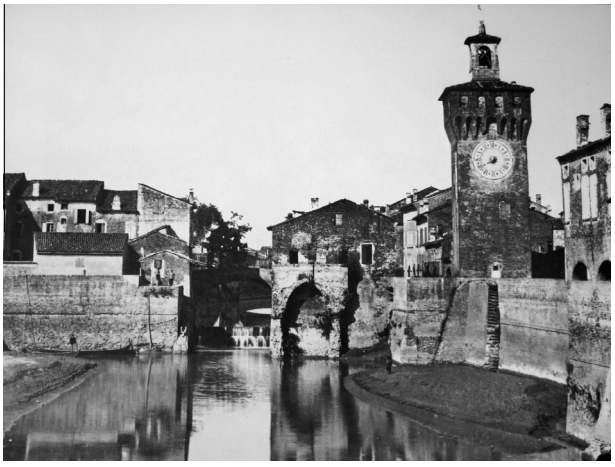

**Fig. 4.** Panaro river near the clock tower, picture taken around 1890 (courtesy G.B. Magni).

In all the analyses carried on, a full three-dimensional (3D) detailed finite element model (FEM) has been developed into both the commercial codes (Strand7 and ABAQUS), starting from the available documentation (photographs and existing drawings as well as direct in situ surveys), to the purpose of evaluating the effect induced by different directions for the seismic load and its distribution. Experimental data available for coeval structures in the same zone and code of practice specifics have been employed to calibrate elastic and inelastic masonry parameters, to be used within the FEM non-linear analyses.

The results confirm an insufficient performance of the tower under horizontal actions and extremely high vulnerability. In particular both vulnerability indices computed in agreement with Italian code of practice (the safety index related to the return period of the seismic demand and capacity of the structure and the acceleration factor based on the soil peak accelerations corresponding to the capacity and the expected demand) are much lower than 1.0, meaning that even a simple linear static analysis is able to put in evidence that the structure did not have the capacity to withstand the design earthquake, whose intensity is similar to the one occurred on the 20th of May.

Dynamic results confirm that the real accelerogram of the 20th May results in severe damages and a collapse of the structure with an evident analogy between the simulated failure mechanism and the real one. However, damages and failure mechanisms obtained with the dynamic analyses appear, as expected, visibly different from those obtained using a static procedure. While pushover simulations envisage a collapse of the tower due to the formation of a combined flexural and shear hinge near the base of the structure, non-linear dynamic analyses exhibit also severe and diffused damage of the tower along the height of the structure.

## 2. Main features of the May 2012 seismic event

The seismic sequence of May 2012 caused a severe damage to many historical masonry buildings and monuments (churches, bell towers, palaces) and precast industrial structures in a large area within the Emilia Region in the Northern part of Italy, among the provinces of Modena, Ferrara and Mantua (see Fig. 5).

Many papers have been recently presented discussing seismological aspects of the event [27–30], as well as the entity of the damage induced on historical buildings, also proposing sophisticated analyses for the numerical interpretation of the behavior of such structures under the seismic sequence occurred [31–33].

Precisely, on May 20, 2012, at 02:03:53 (UTC), the aforementioned area was stricken by an earthquake of magnitude $M_L = 5.9$ (lat 44.890 long 11.230, ipocentral depth 6.3 km).

Accelerograms (N–S, W–E and vertical directions) recorded in Mirandola (the epicenter of the first shake) and post processed elastic spectra along W–E and N–S are reported in Fig. 6.

The main shock was preceded by a $M_L = 4.1$ event on May 19 and followed by four relevant aftershocks with $4.8 < M_L < 5.1$ in the following days: two events with $M_L = 5.1$, one with $M_L = 4.9$ and one with $M_L = 4.8$. Eleven events with magnitude $4.0 < M_L < 4.5$, plus several other minor earthquakes, occurred in the same area between May 20 and May 23, as reported by the Italian Instrumental and Parametric Data-Base (ISIDe) [http://iside.rm.ingv.it/iside/standard/index.jsp].

One of the most impressive practical effects of the earthquake is certainly given by the picture of the Modenesi Tower, also known as the Clock Tower of Finale Emilia and analyzed in this paper, after the main shock. The collapse regarded one half of the tower along the height, with a crack propagating along an almost vertical section passing through the big clock placed near the top (Fig. 1). The impressive image quickly became the symbol of the devastation induced by the seismic event on the cultural heritage. The damage conditions and the precarious equilibrium caused the collapse of the remaining part during the most important shock replicate (M 5.1), which occurred a few hours (at 3:18 PM May 20) after the main shock. The main shock of the sequence in May 2012, like many others with a magnitude between 4 and 5, was originated by earthquakes with epicenters few kilometers far from (the main of May 20 to no more than 10 km to the North-West) the Finale Emilia city center (Fig. 5). The distribution of seismic events with a magnitude greater than 5, located along a broad front with east–west direction, and extension of about 50–60 km, caused the collapse of many other historical buildings and churches in many small towns. The only Finale Emilia, for instance, suffered for serious damages of all the churches, bell towers, and for almost all the aggregates of the old part. Even the fortress was seriously damaged with the total collapse of the main tower (Mastio) and meaningful damages distributed in the upper part of the other three towers. The Fortress Tower is a monument coeval to the Clock Tower, structurally independent from the fortress and slightly higher, but with similar typological and constructive characteristics.

The current seismic zonation map by INGV [Interactive Seismic Hazard Maps, (www.esse1-gis.mi.ingv.it)], employed in the current seismic design codes [19–22], specifies for the epicentral area, with 10% probability of being exceeded in 50 years, an expected maximum horizontal acceleration approximately of 0.15 g on stiff soil, and of 0.22 g on C category soil ($180 \text{ m/s} < V_{S,30} < 360 \text{ m/s}$). Globally, based on historical data, the seismicity of the area can be defined as medium–low. It is remarked that the INGV has proceeded to seismic re-classification of the Padana Plain only in 2003, after the disastrous events of the San Giuliano earthquake in Puglia. Previously, this area was filed as non-seismic, and the first classification of the geographic zone interested by the earthquake events of May 2012 has become legislation only in 2005 [20,21].

In Fig. 7, soil acceleration spectra for soils A and D, according to INGV risk maps are shown (a: horizontal components, b: vertical component), for a returning period of 475 years and 2475 years,

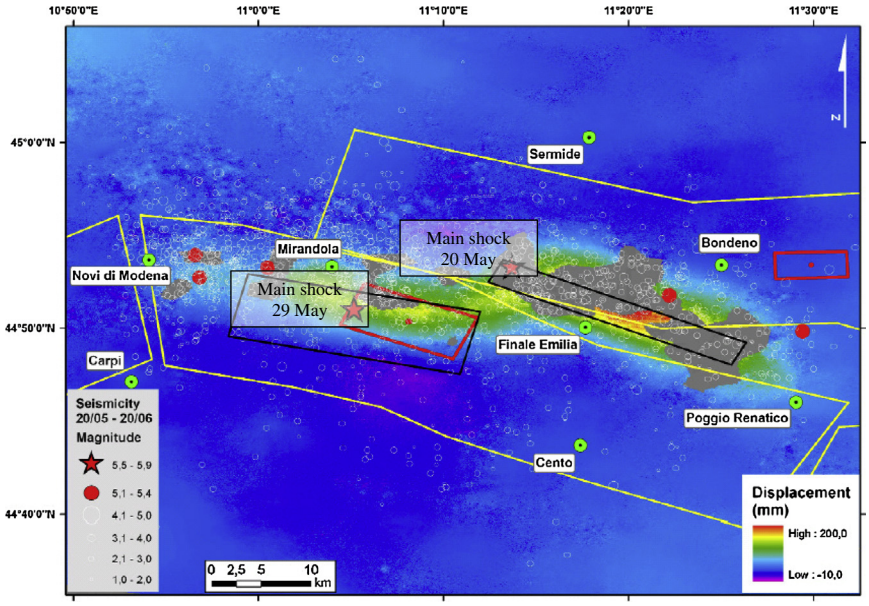


**Fig. 5.** Effects in terms of soil surface deformation produced by the 20th May seismic event, obtained with SAR interferometry technique. Adapted from [27].

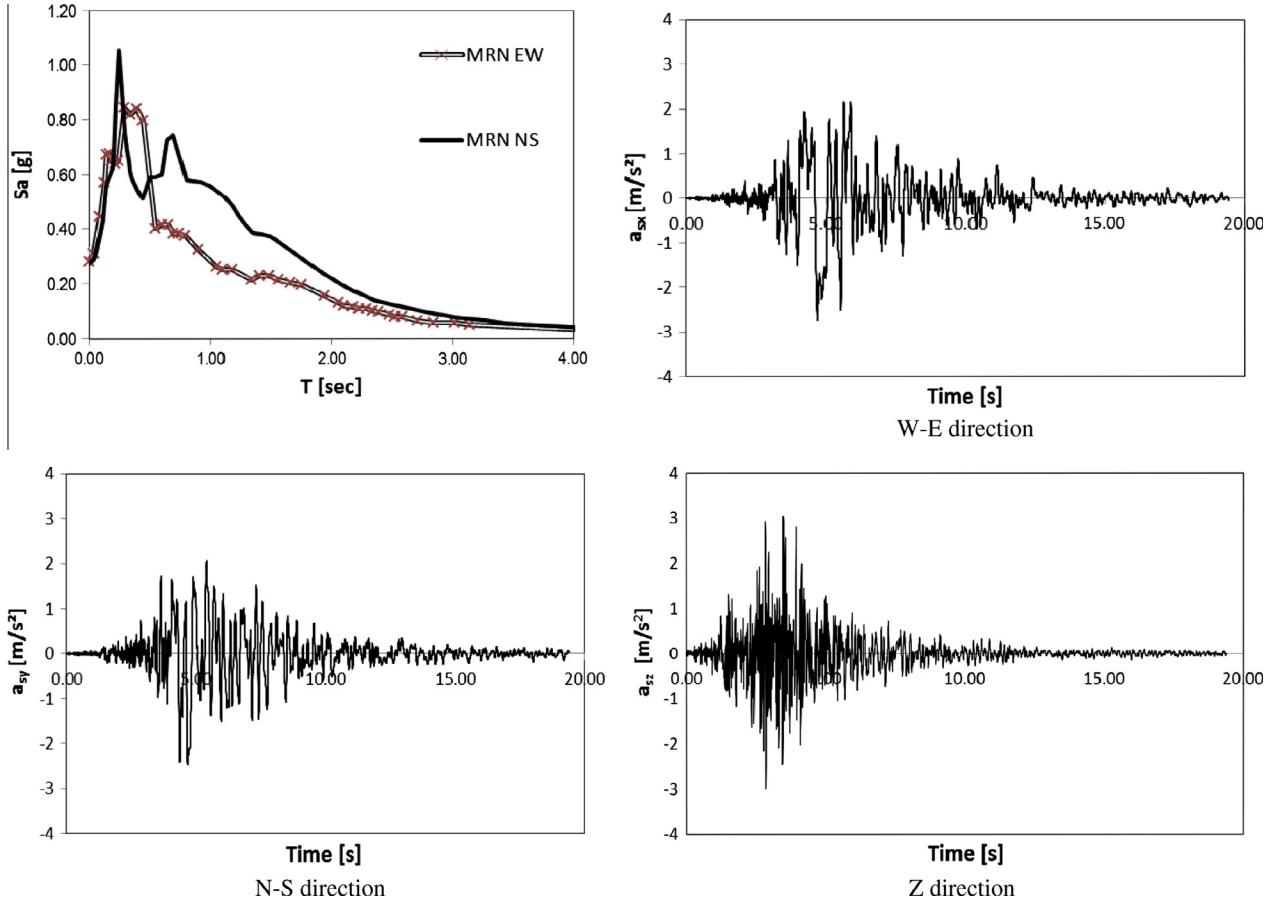


**Fig. 6.** Horizontal Spectra of 20th May seismic event and accelerograms along W–E, N–S and vertical directions.

respectively, compared to the recording at MRN station [first mainshock, Mirandola station]. Apparently the earthquakes are effectively comparable with what expected on the basis of a high return period.

## 3. Material properties

As a matter of fact, masonry is a material which exhibits distinct directional properties due to the mortar joints, acting as planes of weakness. Depending on the level of accuracy and the simplicity desired, it is possible to use the following modeling strategies:

(1) Micro-modeling. Units and mortar in the joints are represented by continuum elements whereas the unit mortar interface is represented by discontinuous elements. To limit the computation effort, in simplified micro-modeling, units are expanded and modeled by continuum elements, whereas the behavior of the mortar joints and unit-mortar interface is lumped in discontinuous elements (e.g. [34]). For the problem at hand, micro-modeling is inapplicable, due to the need of limiting degrees of freedom in the non-linear analyses.

(2) Homogenization (e.g. [35–37]). It replaces the complex geometry of the basic cell using at a structural level a fictitious homogeneous orthotropic material, with mechanical properties deduced from a suitable boundary value problem solved on a suitable unit cell, which generates by repetition the entire structure. For the problem at hand, where multileaf and multi head walls are present, the identification of a unit cell is however questionable and the utilization of orthotropic models would complicate the structural analysis

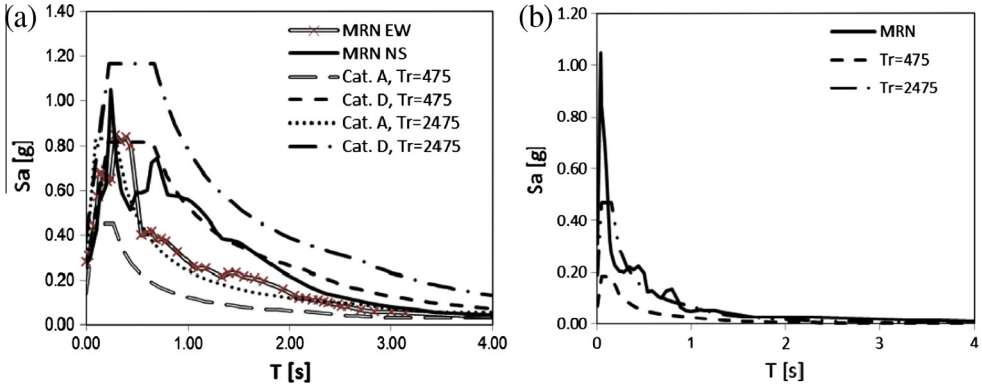


**Fig. 7.** Elastic code of practice spectra compared with that associated to the 20th May seismic event in Finale Emilia. (a): horizontal spectrum; (b): vertical spectrum.

without a sufficiently based hypothesis on the actual texture present. Furthermore, it is expected that orthotropy is a crucial issue for masonry walls loaded within their plane or façade eminently loaded out-of-plane. In this case, the behavior is closer to a squat cantilever beam under vertical flexion. It is therefore preferable the utilization of isotropic materials, also in agreement with existing literature.

(3) Macro-modeling (e.g. [38]). Units, mortar and unit-mortar interface are directly smeared into a continuum (either isotropic or orthotropic), with mechanical properties deduced at the micro-scale by means of experimental data available. This latter approach is probably the most suitable for reliable large scale computations, but it would require a preliminary geometrical and mechanical characterization which, in this specific case, would require costly and time consuming experimental campaigns to fit the several material coefficients needed to perform realistic analyses.

All these features considered, in what follows, isotropic material models are used for masonry, taking into account that the texture is quite irregular and constituted by several layers, with a weak interconnection between internal and external layer. The reason for adopting an isotropic material stands in the impossibility to evaluate the many parameters necessary for anisotropic materials in the inelastic range, in absence of ad-hoc experimental characterization. In addition, it is worth noting that for towers the most important parameters to set are shear and inelastic behavior along the vertical direction, being such structures mainly characterized by vertical bending. As many homogenization studies shown [35,36], for masonry textures with continuous bed joints, homogenized vertical stress/moment and shear strength are almost exclusively dependent on mortar mechanical properties. Finally it is worth noting that commercial codes rarely put at disposal to users anisotropic mechanical models suitable to describe masonry with regular texture in the non-linear regime.

Three materials are present in the model, namely ordinary masonry (external and internal walls and vaults), infill (disposed over the vaults as commonly done in building practice to both increase vaults strength and to realize planar floors) and timber beams (belfry sustaining frame).

According to Italian Code NTC2008 [19], Chapter 8, and subsequent Explicative Notes [22], the mechanical properties to assume for the masonry material depend on the so called knowledge level LC, which is related to the so called Confidence Factor $F_c$. There are three LCs, labeled from 1 to 3, related to the level of knowledge that one has on the mechanical and geometrical properties of the structure. LC3 is the maximum, whereas LC1 is the minimum. For the case at hand, in absence of specific in situ test results, a LC1 level is assumed.

$F_C$ summarizes the level of knowledge regarding the structure and the foundation system, from a geometric and mechanical point of view. It can be determined defining different partial confidence factors $F_{Ck}$ ($k = 1, 4$), on the base of some numerical coefficients presents in the Italian Code (Table 4.1 Italian Line Guides). Due to the limited level of knowledge achieved in this case, the highest confidence factor was used, $F_C = 1.35$.

After visual inspections, values adopted for cohesion and masonry elastic moduli are taken in agreement with Table C8A.2.1 of the Explicative Notes [22], assuming a masonry typology constituted by clay bricks (approximate dimensions $210 \times 52 \times 100\ mm^3$) with very poor mechanical properties of the joint and quite regular courses.

Elastic and inelastic material properties utilized in both the linear and non-linear pushover analyses are summarized in Tables 1–3 (these latter values for the dynamic analyses). With the lowest knowledge level LC (confidence factor $F_C = 1.35$), Italian code requires to select in Table C8A.2.1, the lower bound values for strength and the average between lower and upper bound for elastic moduli.

Pushover analyses are conducted within Strand 7 [25] with an elastic perfectly plastic material obeying a Mohr–Coulomb failure criterion. A friction angle equal to 20 degrees is assumed, again in agreement with the Italian code. The utilization of perfectly plastic materials is allowed by the Italian Guidelines when masonry is modeled with 2D and 3D finite elements, i.e. where the drop of the pushover curve for the reduction to a 1DOF system with the area equivalence is hardily reproducible. In this case, the Italian Guidelines recommend carrying on the analyses up to "meaningful displacement", which reasonably may be associated to an activation of the failure mechanism.

The dynamic analysis conducted by means of ABAQUS [26] is performed assuming a concrete damage-plasticity (CDP) material model for masonry, already available in the standard software package, which allows for a reliable non-linear behavior investigation of the tower under load–unload conditions. Although the model is specifically suited for a fragile isotropic material (as is the case of concrete), its basic constitutive laws can be adapted for reproducing masonry properties in the inelastic range. The "concrete model" allows for modeling materials with distinct tensile and compressive strength, as the case of masonry, with distinct damage parameters in tension and compression, see also Fig. 8.

The plasticity-based damage model adopted in dynamic analyses, assumes that the main two failure mechanisms are tensile cracking and compressive crushing. Under cyclic loading conditions the degradation mechanisms involve the opening and closing of previously formed cracks. The experimentally observed effect, according to which there is some recovery of the elastic stiffness as the stress changes sign, is called "unilateral effect". This phenomenon, which is usually more pronounced as the stress state changes from tension to compression, causing tensile cracks to close, has been modeled by two distinct damage variables, one in compression and one in tension, which are assumed to be function of the plastic strains. These variables may assume values from zero (undamaged material) to one, which represents total loss of stiffness.

The strength domain is a Drucker Prager DP surface modified with an ad-hoc $K_c$ parameter, which distorts the DP surface in the deviatoric plane from a circle to a surface more similar to a Mohr–Coulomb one. $K_c$ physically represents the ratio between distance from the hydrostatic axis of the maximum compression and tension respectively. In the simulations $K_c$ has been kept equal to 2/3, a value suggested by the user's Guide to well approximate a Mohr–Coulomb failure criterion.

A regularization of the tensile corner is also adopted in the model, approximating in the $p$–$q$ plane the line representing the DP domain with a hyperbola. Regularization is practically obtained in the model with a further correction parameter, referred to as eccentricity, expressing the rate at which the plastic flow potential approaches the linear Drucker–Prager function at high confining pressure stress. The 0.1 default value was adopted. Smaller values may cause convergence problems when the material is subjected to low confining pressures because of the very tight curvature the flow potential possesses locally where it intersects the hydrostatic axis.

**Table 1**
Mechanical properties adopted for masonry and vaults infill.

| | $f_m$ (N/cm$^2$) | $\tau_0$ (N/cm$^2$) | $E$ (MPa) | $G$ (MPa) | $w$ (kN/m$^3$) |
|---|---|---|---|---|---|
| Masonry with clay bricks and poor mortar | 240–400 | 6–9,2 | 1200–1800 | 400–600 | 18 |
| Infill | 74 | 3,7 | 689 | 296 | 16 |

**Table 2**
Compression mono-axial curve depurated from the elastic part.

| Stress (MPa) | Inelastic strain |
|---|---|
| 2.4 | 0 |
| 1.9 | 0.005 |
| 1.9 | 0.01 |
| 1.8 | 0.1 |

**Table 3**
Tensile mono-axial curve depurated from the elastic part.

| Stress (MPa) | Inelastic strain |
|---|---|
| 0.17 | 0 |
| 0.0005 | 0.003 |
| 0.0005 | 0.1 |

Such parameter results in a slight decrease of the tensile strength, with an error lower than 5%.

A non associated behavior is assumed for the elasto-plastic deformation part. Dilatance angle $\psi$ of the elasto-plastic part of the inelastic deformation has been kept equal to 10°, in agreement with some experimental data by van der Pluijm [39] in presence of moderate pre-compression levels.

A value equal to 1.16 describing the ratio between the biaxial and mono-axial compression strength has been adopted, again in agreement with consolidated literature regarding the behavior of clay-brick masonry in compression, see [40].

The uniaxial inelastic behavior due to the damage part is evaluated with a multi-linear softening model in both tension and compression, with strains depurated from the elastic part.

Values adopted in the model are summarized in Tables 2 and 3 for the compressive and tensile behavior respectively.

Damage parameters $d_t$ e $d_c$ in tension and compression enter, as usual, into the uniaxial Hook's law as $\sigma_t = (1 - d_t)E_0(\varepsilon_t - \varepsilon_t^{ple})$ and $\sigma_c = (1 - d_c)E_0(\varepsilon_c - \varepsilon_c^{ple})$ where $\sigma_t$ and $\sigma_c$ are uniaxial tensile and compressive stresses, $E_0$ is the initial elastic modulus, $\varepsilon_c$ and $\varepsilon_t$ are the total strain in compression and tension and $\varepsilon_c^{ple}$ ($\varepsilon_t^{ple}$) are the total plastic deformation in compression (tension).

In view of the fact that masonry compressive strength is for the case under study quite high and crushing occurs for compressive stresses exceeding 5–8 MPa in coeval structures where an experimental determination of the mechanical properties was possible [41], the simplified choice to assume a pure elasto-plastic behavior in compression is made. In tension, a linear damage mode is adopted ($d_t$ = 0.95 for a plastic deformation equal to 0.3%).

Vaults infill (density 1600 kg/m$^3$) is finally modeled with an elastic material having very weak elastic properties (Young modulus equal to 689 MPa and Poisson's ratio equal to 0.16).

## 4. FE 3D model and loads applied

Loads applied when dealing with the pushover analysis are: masonry self-weight, bell cell weight, wooden and masonry floors weight (dead and live loads) and seismic action incremented up to failure. The behavior of the structure is investigated along the principal directions *X* and *Y* (see Fig. 9 for axes direction), only with positive verse (+). Rigorously, due to the small geometrical asymmetries of the structure, the response along *X*− and *Y*− directions should be also considered. However, authors experienced negligible differences and only results for *X*+ and *Y*+ are here discussed for the sake of conciseness.

The Italian code [19] prescribes the evaluation of the load carrying capacity by means of two configurations of horizontal forces: the first provides a distribution of forces derived by the assumption of a linear variation of acceleration along the height (Group 1, G1) while for the second it is assumed a constant acceleration (Group 2, G2). As prescribed by the Instructions for NTC 2008 [22] the first distribution of forces of Group 1 and Group 2 can be applied independently of the participating mass activated by the first mode. Authors experienced that G2 distribution is systematically less safe for the cases analyzed, i.e. provides larger failure horizontal accelerations.

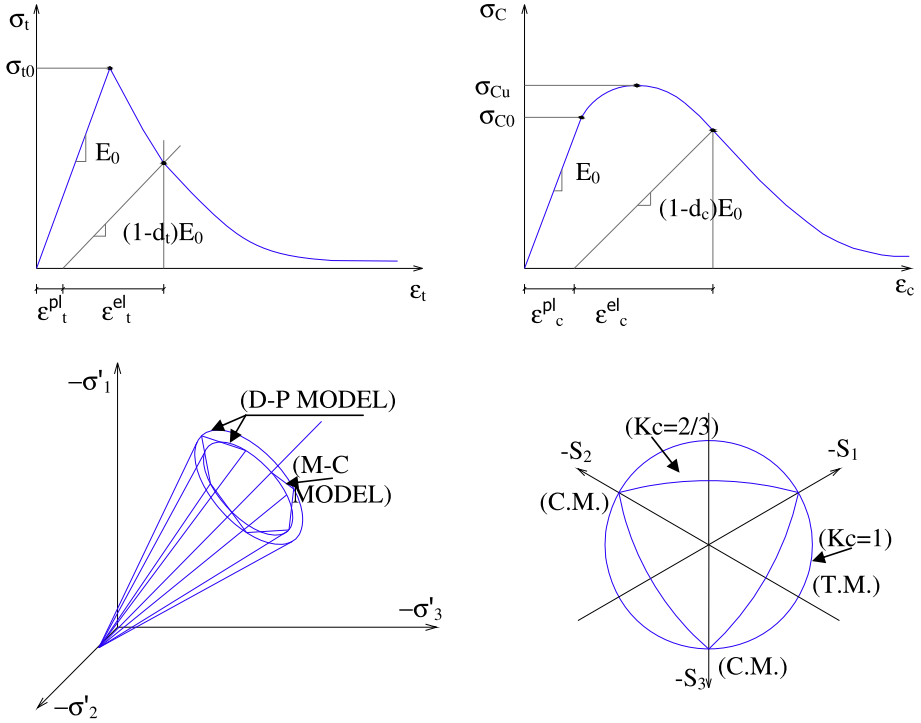


**Fig. 8.** ABAQUS material non-linear behavior in uniaxial tension and compression to analyze the bell tower under non-linear dynamic loads.

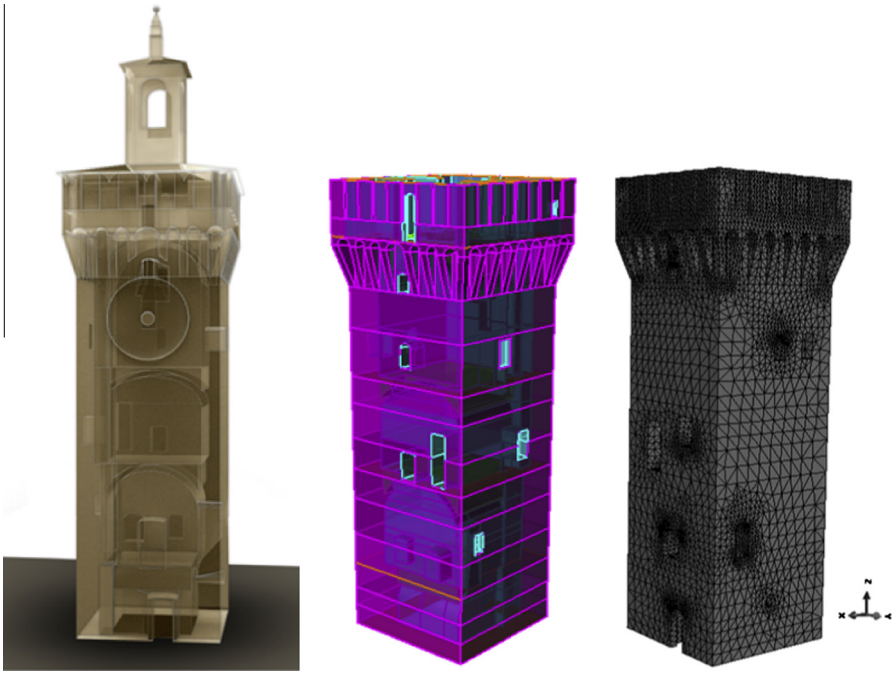

**Fig. 9.** Rynocheros 3D geometric model and FE discretization of the tower by means of four noded tetrahedron elements (24,285 brick elements and 7161 nodes).

When dealing with the non-linear dynamic analysis, the actual accelerogram of the 20th May main shock registered in Mirandola station is utilized for the analyses, provided that the peak accelerations are scaled on Finale Emilia basing on INGV iso-PGA maps and E–W and N–S components are suitably trigonometrically combined according to the actual position of the tower in plan with respect to the wave front.

## 5. Numerical results

In this section, results obtained by means of all the models proposed (3D static, modal, pushover, limit and dynamic non-linear analyses) are shown and discussed in detail, starting from the preliminary (standard) static and modal analysis and concluding with the non-linear dynamic outcomes.

### *5.1. Static analysis under gravity loads and modal analysis*

A preliminary static analysis under gravity loads is performed assuming a "quasi" no-tension material model (Mohr–Coulomb failure criterion with cohesion equal to 0.03 MPa and friction angle 20°) for masonry and progressively increasing the vertical loads up to their actual value.

The resultant vertical stress distribution color patch is represented in Fig. 10. As can be noted, the pre-compression exhibits some peaks at the first floor level of about 0.9 MPa, with positive values of stress in correspondence of the vaults. However, on average, vertical stress maintains generally lower than 0.4 MPa, a value indicating that the state of stress at the base for gravity loads is far away from the ultimate compressive strength, meaning also that the tower exhibits a satisfactory behavior under self weight.

In order to assess a global seismic response with conventional procedures, a modal analysis is also performed on the same 3D FEM model used for the static analysis, even though the ability of such a model to represent the actual behavior of the construction is limited, due to the tendency of masonry structures to alter significantly their behavior in response to dynamic seismic action. Moreover the knowledge of eigen-values, eigen-modes and the corresponding activated mass is required for the determination of the shape of the horizontal load distribution to utilize within the pushover procedure.

The structure is regular in plane but irregular in elevation, due to some sudden changes of thickness of the walls (and hence of mass) and the presence of the bell cell.

The behavior factor q is calculated as prescribed by the Guidelines provided by the Italian Ministry for the Cultural Heritage [23], taking into account the irregularity in elevation and results equal to 2.8. The spectrum adopted for the modal analysis is related to a return period of 475 years and a soil type C and D, with use class II; the parameters which characterize the spectrum are defined according the Italian Norms (NTC 2008). For modal analyses, only elastic properties are needed: they are summarized in Table 1 and are taken again in agreement with the Italian code.

Periods and excited mass in *X* and *Y* directions from modal analysis, together with the activated mass percentage are listed in Table 4. In addition, the modal deformed shapes corresponding to the first six modes are depicted in Fig. 11. As usually occurs for towers, it is worth noting that the largest excited mass in *X* direction corresponds to the first mode and approximately represents the 45% of the total mass, whereas in *Y* direction corresponds to the second mode and it is equal to around 46%. It is not surprising that the behaviors along *X* and *Y* directions are very similar, in view of the quasi square planar section of the structure. Small differences depend on some minor geometric irregularities (as openings) and internal vaults distributions.

The resulting response conventionally represents the behavior of the structure during the earthquake. The eigenvalue analysis is extremely useful in light of the pushover simulations to perform later. Indeed, to reduce the structure to a 1DOF system, the Italian code requires the knowledge of the normalized fundamental mode displacement vector.

A comparison of all the results with a cantilever beam model is also possible in this case – except for the torsional third mode – and may be useful for practical purposes, to confirm that the natural frequencies of the tower may be evaluated with acceptable

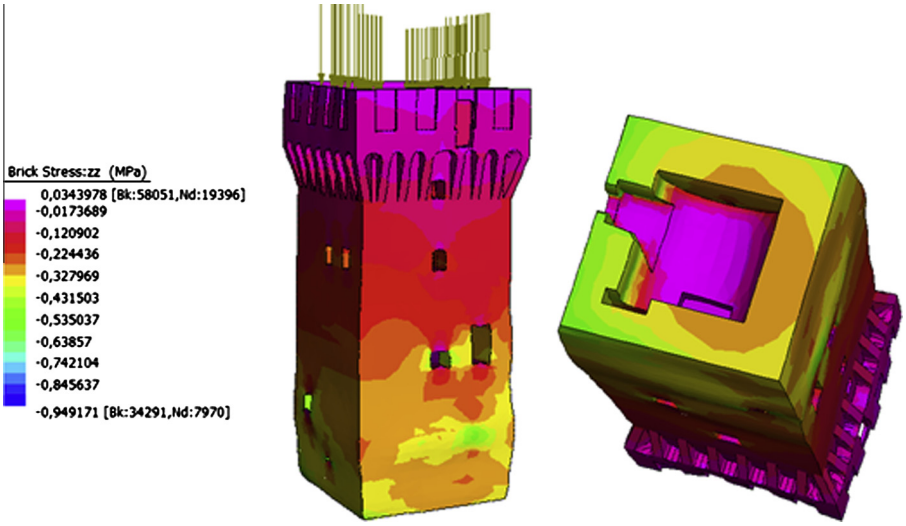


**Fig. 10.** Results of the static analyses under gravity loads, elasto-plastic material.

**Table 4**
Vibration modes, frequencies, periods and participating masses.

| Modes | Frequency, $f$ (Hz) | Period, $T$ (s) | $m_{i,x}$ (%) | $m_{i,y}$ (%) | $m_{i,z}$ (%) |
|---|---|---|---|---|---|
| 1 | 2.38 | 0.4194 | 45.42 | 15.19 | 0.00 |
| 2 | 2.43 | 0.4122 | 15.39 | 46.45 | 0.00 |
| 3 | 5.95 | 0.1680 | 0.01 | 0.13 | 0.00 |
| 4 | 9.10 | 0.1099 | 0.57 | 19.37 | 0.04 |
| 5 | 9.52 | 0.1050 | 19.87 | 0.76 | 0.31 |
| 6 | 11.02 | 0.0908 | 0.11 | 0.02 | 77.14 |
| 7 | 14.14 | 0.0707 | 0.22 | 0.01 | 0.01 |
| 8 | 15.30 | 0.0654 | 0.73 | 0.00 | 0.00 |
| 9 | 16.84 | 0.0594 | 0.00 | 0.04 | 0.00 |
| 10 | 17.88 | 0.0559 | 0.04 | 0.71 | 0.00 |
| 11 | 18.22 | 0.0549 | 0.01 | 3.61 | 0.00 |
| 12 | 19.45 | 0.0514 | 0.28 | 0.25 | 0.00 |
| 13 | 1.96E+01 | 0.0511 | 2.11 | 0.04 | 0.01 |
| 14 | 1.99E+01 | 0.0501 | 1.00 | 0.43 | 0.00 |
| 15 | 2.12E+01 | 0.0471 | 0.81 | 0.02 | 0.00 |
| 16 | 2.22E+01 | 0.0450 | 0.10 | 0.19 | 0.02 |
| 17 | 2.26E+01 | 0.0442 | 0.03 | 0.04 | 0.00 |
| 18 | 2.35E+01 | 0.0425 | 0.02 | 0.04 | 0.01 |
| 19 | 2.51E+01 | 0.0399 | 1.11 | 0.12 | 0.00 |
| 20 | 2.53E+01 | 0.0395 | 0.01 | 0.03 | 0.02 |
| 21 | 2.55E+01 | 0.0392 | 1.22 | 0.00 | 0.03 |
| 22 | 2.58E+01 | 0.0388 | 0.00 | 1.17 | 0.01 |
| 23 | 2.61E+01 | 0.0384 | 0.12 | 0.02 | 0.10 |
| 24 | 2.62E+01 | 0.0382 | 0.29 | 0.88 | 0.00 |
| 25 | 2.69E+01 | 0.0372 | 0.01 | 0.17 | 0.00 |
| Total participating mass | | | 89.48 | 89.70 | 77.71 |

accuracy even without the utilization of complex 3D FE analyses. In particular the frequency of the tower, assuming a cantilever beam hypothesis is given by the following formula:

$$f_i = \frac{\alpha_i}{2\pi L^2}\sqrt{\frac{EI}{\mu A}} \tag{1}$$

where $\mu$ (=1800 kg/m$^3$) is the average density of the structure, $L$ the height (22.47 m without the belfry), $E$ (1500 N/mm$^2$) is the Young modulus, $A$ (=24 m$^2$) and $I$ (=150 m$^4$) are the equivalent base cross section area and inertia moment (taking into account in an approximate way the average thickness and the many irregularities of the tower), and $\alpha_i$ is a coefficient associated to the $i$th mode inspected. For $i = 1$ $\alpha_i = 3.5156$.

The inertia moments along $X$ and $Y$ direction are almost equal, thanks to the quasi square cross section of the tower. Therefore, in the cantilever beam approach they are kept equal.

With such hypotheses, from (1) a period $T$ equal to 0.3954 s is obtained, in very good agreement with FEM simulations.

Authors experienced that the mass of the belfry (constituted by very thin perimeter walls of 15 cm carried by a complex wooden frame working with prevailing bending and a small bell) in practice, does not influence the period of the tower. While the belfry weight may be easily taken into account in the FE models, within the cantilever beam assumption, it is obviously disregarded. On the other hand, it is worth noting here that the bell cell is highly perforated and both the weight and the inertia of the upper part of the tower cannot be modeled with sufficient accuracy within the context of formula (1). In addition, in formula (1) some other important structural aspects typical of the tower under consideration, such as internal vaults, openings, and stairs are disregarded.

### 5.2. Equivalent static analysis under horizontal loads

The equivalent static analysis (ESA) was carried out in accordance with Section 5.4.4 of the Guidelines [23], adopting a distribution of horizontal forces on the nodes of the mesh proportional to the product $W_i z_i$, being $W_i$ the weight associated to the $i$th node and $z_i$ its vertical position. When evaluating the resultant horizontal force as $F_h = 0.85\ S_e(T_1)\ W/(qg)$, reference was made to the elastic response spectrum $S_e$ provided by the NTC 2008 [19], reduced by the behavior factor $q = 2.8$ suggested by the above Guidelines in the case of stiffness irregularities along the height. The spectral ordinate corresponding to the fundamental period $T_1 = 0.419$ s was alternately referred to the use classes II and III and to the categories of foundation soil C and D. In fact, the use class of the tower is governed by the use of the tower (civic tower) and those of the nearby buildings. Moreover, with reference to the category of foundation soil, penetration tests conducted not far from the structure under consideration and measurements of the velocity of shear waves, indicate a soil which can be classified on the borderline between the categories C and D. On the other hand, the presence of the Panaro river – before its deviation – in a position adjacent to the tower, suggests to consider for the tower a soil with very low mechanical properties (soil D).

According to the Italian Guidelines, it is necessary to compare the acting bending moments on different transversal sections, within the application of equivalent static loads and under the hypotheses of class use and soil done, with the resisting ones.

For towers with rectangular section, FEM may be avoided and simplified formulas could be adopted according to Italian

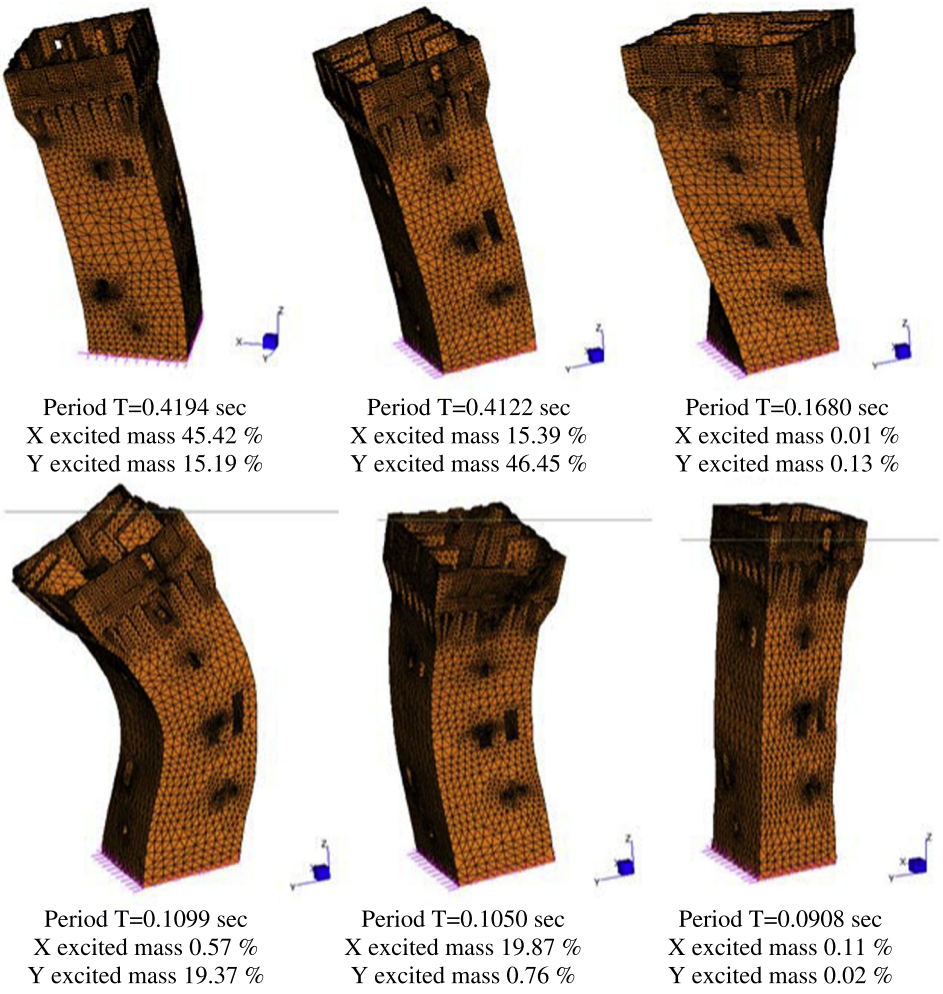


**Fig. 11.** Modal eigenvalues analysis.

Guidelines specifics. Under the hypothesis that the normal pre-compression does not exceed 0.85 $f_d A_s$, the ultimate bending moment of a masonry rectangular sections is:

$$M_u = \frac{\sigma_0 A}{2}\left(b - \frac{\sigma_0 A}{0.85 a f_d}\right) \tag{2}$$

where $a$ is the transversal edge length of the section, $b$ the longitudinal length edge, $A$ the section area, $\sigma_0 = W/A$ the average pre-compression ($W$: tower weight above the section considered) and $f_d$ the design compressive strength.

External moments, within a cantilever beam hypothesis (subdivided into $n$ elements), may be evaluated at the generic section $j$ as:

$$M_j = F_e z_j$$
$$z_j = \frac{\sum_{i=1}^{j} z_i^2 W_i}{\sum_{k=1}^{n} z_k W_k} \tag{3}$$

With $F_e = 0.85\ S_d(T_1)W/g$ ($S_d$ spectrum, $T_1$ first period of the structure, $g$ gravity acceleration).

Since a detailed FEM discretization is already at disposal to the authors, the simplified approach is avoided and external moments are estimated by integration of the internal nodal vertical stresses on prescribed transversal sections, with the prescribed horizontal loads distribution.

In a similar way, resisting bending moments are evaluated with an ad hoc numerical model on the 13 different transversal sections shown in Fig. 9, where a no-tension material model is adopted for masonry.

The resultant distributions of resisting and acting bending moments along the height of the structure are depicted in Fig. 12. In particular in subfigure a the case with use class II and Italian code spectrum is represented. Fig. 12b refers to use class III and Fig. 12c to the 20th May 2012 spectrum. Two acting bending moment distributions per figure are represented in Fig. 12a and b, corresponding to soil C and D.

As can be noted, in all cases the lower part, up to a height approximately equal to 7 m, of the structure exhibits insufficient strength for flexural actions. The presence of some openings in the lower part weakens further the transversal section decreasing the resistance against flexural actions, which obviously reach the maximum on the fixed base. When dealing with Italian code spectrum, the maximum percentage difference between applied and resistant moments (equal to 39%) is registered along $Y$ direction, obviously for use class III and soil type D. For the 20th May 2012 spectrum, the percentage difference slightly increases up to 43%. A synopsis of resistant and acting bending moments on the 13 sections considered, as well as the deficiency strength in the lower part of the structure measured as percentage difference between resistant and acting values is reported in Table 5 (Italian Code spectra) and Table 6 (20th May seismic event).

*5.2.1. Evaluation of the seismic safety index and acceleration factor*

A preliminary simplified analysis may be conducted on the tower under consideration by means of the evaluation of the

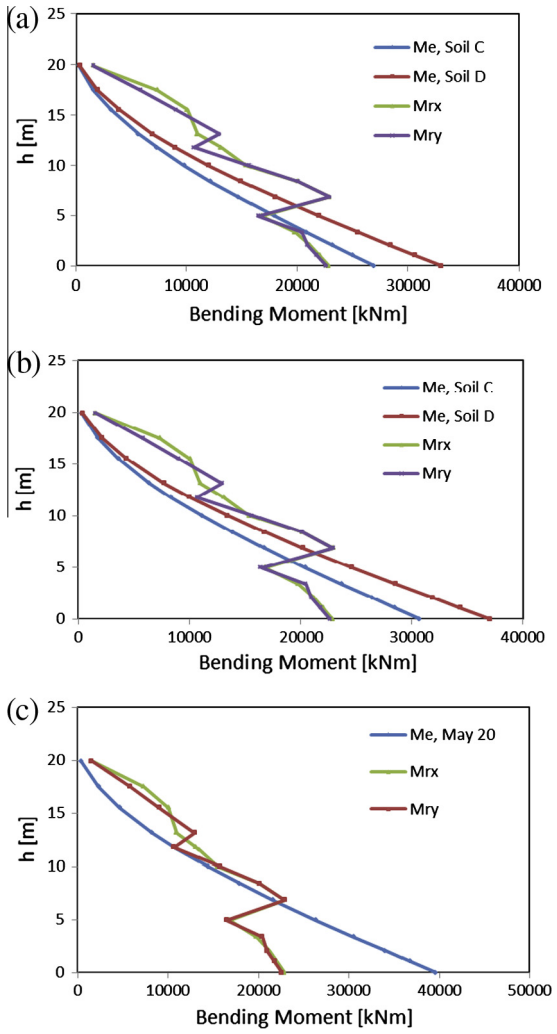


**Fig. 12.** Static analysis according to the Italian Guidelines on architectural heritage. (a): use class II, Italian code spectrum. (b): use class III, Italian code spectrum. (c): 20th May 2012 spectrum.

vulnerability index $I_s$ according to the Italian Guidelines on cultural heritage buildings [23].

The Guidelines assume as safety index the ratio:

$$I_{S,SLV} = \frac{T_{SLV}}{T_{R,SLV}} \tag{4}$$

where $T_{SLV}$ is the return period for the ultimate limit state SLV (life safeguard) and $T_{R,SLV}$ is the reference return period. Clearly an index greater than one corresponds to a safe state for the tower under consideration.

Being the seismic safety index $I_S$ based on return periods of the seismic demand and the capacity of the structure, it allows also a direct evaluation of the eventually present vulnerability of the structure during the time.

The acceleration factor is the ratio between soil peak accelerations corresponding to the capacity and the expected demand:

$$f_{a,SLV} = \frac{a_{SLV}}{a_{g,SLV}} \tag{5}$$

where $a_{SLV}$ is the soil acceleration leading to the SLV ultimate state and $a_{g,SLV}$ is the acceleration corresponding to the reference return period. This latter is a purely mechanical parameter, which may be useful for an evaluation of the weakness of the structure in terms of strength.

In order to evaluate the acceleration of the response spectrum corresponding to the instant where SLV limit state is reached on the $i$th section, taking into account the reduction induced by the confidence factor, the following equation is used:

$$S_{e,SLV,i}(T_1) = \frac{qgM_{R,i}\sum_{k=1}^{13} z_k W_k}{0.85WF_C\left(\sum_{k=1}^{13} z_k^2 W_k - z_i \sum_{k=1}^{13} z_k W_k\right)} \tag{6}$$

where $q$ is the behavior factor, $g$ the gravity acceleration, $M_{R,i}$ is the resistant bending moment on the $i$th section, $z_k$ and $W_k$ are the height and the weight in correspondence of the $k$th section, respectively, $W$ the total weight, $F_C$ the confidence factor and $z_i$ the height of the $i$th section with respect to the base.

When the transversal section where the minimum value of $S_{e,SLV}$ occurs is identified, the return period $T_{SLV}$ of the corresponding seismic action may be found by means of an iterative procedure with linear interpolation. The procedure utilizes available data in the Italian Code NTC appendix which, for each point of the reference topographic grid, furnishes the values of the spectra ($a_g$, $F_0$ e $T_c^*$) for return periods equal to 30, 50, 72, 101, 140, 201, 475, 975 and 2475 years.

For all the cases analyzed, the minimum spectral acceleration is obtained in correspondence of the base section.

Finally, to evaluate the maximum soil acceleration corresponding to the minimum spectral acceleration, the following equation is used:

$$a_{SLV} = \begin{cases} \frac{S_{e,SLV}}{SF_0} & T_B \leqslant T_1 \leqslant T_C \\ \frac{S_{e,SLV}}{SF_0}\frac{T_1}{T_C} & T_C \leqslant T_1 \leqslant T_D \end{cases} \tag{7}$$

**Table 5**
Values of the resistant and applied bending moments evaluated with the Italian code spectrum.

| Level (m) | $M_{Rx}$ (kNm) | $M_{Ry}$ (kNm) | $M_{e.c,II}$ (kNm) | $\Delta x$ (%) | $\Delta y$ (%) | $M_{e.d,II}$ (kNm) | $\Delta x$ (%) | $\Delta y$ (%) | $M_{e.c,III}$ (kNm) | $\Delta x$ (%) | $\Delta y$ (%) | $M_{e.d,III}$ (kNm) | $\Delta x$ (%) | $\Delta y$ (%) |
|---|---|---|---|---|---|---|---|---|---|---|---|---|---|---|
| 0 | 22,832 | 22,584 | 26,955 | 15 | 16 | 33,032 | 31 | 32 | 30,681 | 26 | 26 | 37,001 | 38 | 39 |
| 1.04 | 21,998 | 21,759 | 25,025 | 12 | 13 | 30,666 | 28 | 29 | 28,484 | 23 | 24 | 34,352 | 36 | 37 |
| 2.03 | 21,147 | 20,918 | 23,196 | 9 | 10 | 28,426 | 26 | 26 | 26,403 | 20 | 21 | 31,842 | 34 | 34 |
| 3.35 | 19,752 | 20,430 | 20,789 | 5 | 2 | 25,476 | 22 | 20 | 23,663 | 17 | 14 | 28,538 | 31 | 28 |
| 4.96 | 16,762 | 16,439 | 17,936 | 7 | 8 | 21,979 | 24 | 25 | 20,415 | 18 | 19 | 24,621 | 32 | 33 |
| 6.85 | 22,893 | 22,893 | 14,698 | | | 18,012 | | | 16,730 | | | 20,176 | | |
| 8.39 | 20,083 | 20,083 | 12,192 | | | 14,941 | | | 13,878 | | | 16,737 | | |
| 9.98 | 15,401 | 15,679 | 9809 | | | 12,021 | | | 11,165 | | | 13,466 | | |
| 11.77 | 13,139 | 10,679 | 7332 | | | 8985 | | | 8345 | | | 10,065 | | |
| 13.12 | 10,999 | 12,984 | 5644 | | | 6916 | | | 6424 | | | 7748 | | |
| 15.51 | 10,073 | 9051 | 3191 | | | 3910 | | | 3632 | | | 4380 | | |
| 17.5 | 7351 | 5839 | 1584 | | | 1941 | | | 1803 | | | 2174 | | |
| 19.89 | 1569 | 1569 | 275 | | | 336 | | | 312 | | | 377 | | |

**Table 6**
Values of the resistant and applied bending moments evaluated with the 20th May seismic event spectrum.

| Level (m) | $M_{Rx}$ (kNm) | $M_{Ry}$ (kNm) | Me.20 (kNm) | $\Delta x$ (%) | $\Delta y$ (%) |
|---|---|---|---|---|---|
| 0 | 22,832 | 22,584 | 39,584 | 42 | 43 |
| 1.04 | 21,998 | 21,759 | 36,750 | 40 | 41 |
| 2.03 | 21,147 | 20,918 | 34,065 | 38 | 39 |
| 3.35 | 19,752 | 20,430 | 30,530 | 35 | 33 |
| 4.96 | 16,762 | 16,439 | 26,340 | 36 | 38 |
| 6.85 | 22,893 | 22,893 | 21,585 | | |
| 8.39 | 20,083 | 20,083 | 17,905 | | |
| 9.98 | 15,401 | 15,679 | 14,406 | | |
| 11.77 | 13,139 | 10,679 | 10,767 | | |
| 13.12 | 10,999 | 12,984 | 8288 | | |
| 15.51 | 10,073 | 9051 | 4686 | | |
| 17.5 | 7351 | 5839 | 2326 | | |
| 19.89 | 1569 | 1569 | 403 | | |

**Table 7**
Values of the safety index by Italian Guidelines and acceleration factors found in the different cases.

| Use class | Soil type | Seismic load direction | $S_{e,slv}(T_1)$ (g) | $T_{slv}$ (anni) | $I_s$ | $a_{slv}$ (g) | $f_a$ |
|---|---|---|---|---|---|---|---|
| II | C | *X* | 0.355 | 169.1 | 0.356 | 0.093 | 0.624 |
| II | C | *Y* | 0.351 | 165.1 | 0.348 | 0.092 | 0.617 |
| II | D | *X* | 0.355 | 114.2 | 0.241 | 0.077 | 0.518 |
| II | D | *Y* | 0.351 | 112.1 | 0.236 | 0.076 | 0.513 |
| III | C | *X* | 0.355 | 179.2 | 0.252 | 0.096 | 0.544 |
| III | C | *Y* | 0.351 | 175.1 | 0.246 | 0.095 | 0.538 |
| III | D | *X* | 0.355 | 123.1 | 0.173 | 0.080 | 0.454 |
| III | D | *Y* | 0.351 | 120.8 | 0.170 | 0.079 | 0.450 |

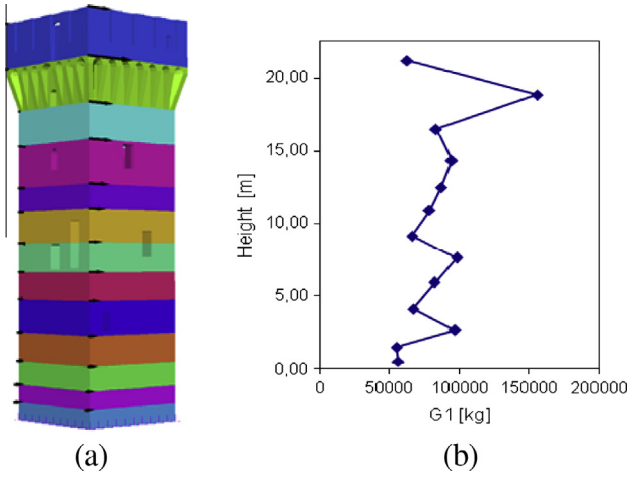


**Fig. 13.** Simplified G1 force distribution (a) and mass distribution along tower height (b).

where $T_B$, $T_C$, $T_D$ are characteristic periods of the response spectrum, assumed in agreement with the Italian code and $S$ is coefficient which takes into account the soil and topographical categories. The final values of $I_S$ and $f_a$ are reported in Table 7.

As it is possible to notice, the safety index $I_S$ is always largely lower than 1. For D type soil and use class III obviously the situation becomes very critical, with the minimum value of $I_S$ equal to 0.17. The tower is slightly more vulnerable along *Y* direction, probably for the geometrical irregularity induced by internal vaults disposition.

Furthermore, it is worth underlining that the case with $I_S$ maximum (use class II, C soil type and seismic load along *X* direction) is associated with an acceleration $a_{SLV}$ equal to 0.093 g, much lower

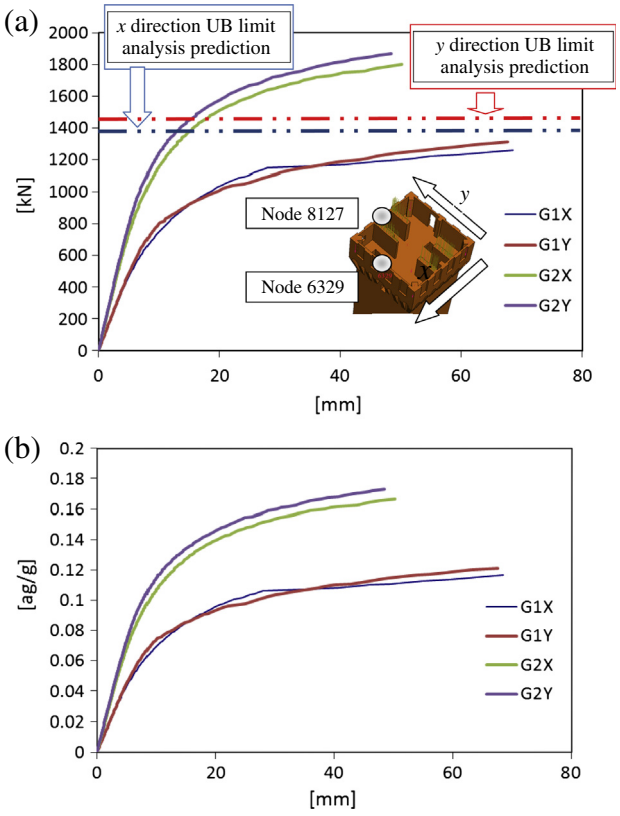


**Fig. 14.** Pushover curves obtained for distributions G1 and G2. (a): total base shear vs control node horizontal displacement. (b): acceleration *ag*/*g* vs control node horizontal displacement.

than the PGA registered during the 20th May shake (roughly equal to 0.25 g). Finally, it is noted that the acceleration factor exhibits an average value equal to 0.53, meaning that the soil acceleration associated to the collapse of the tower (SLV state) is approximately one half the acceleration required for the reference return period.

### 5.3. 3D pushover analyses

In the last few years, simplified procedures have been proposed for the non-linear static analysis of masonry structures. These methods, generally known as pushover analyses, have recently assumed a large relevance, especially for the assessment of existing buildings, also in light of code of practice requirements. Basically, a computational model of the structure is loaded up with a proper distribution of horizontal static loads, which are gradually increased with the aim of "pushing" the structure into the non-linear field. The resulting response conveniently represents the envelope of all the possible structural responses, and can so be used to replace a full non-linear dynamic analysis.

Here full 3D pushover analyses are performed on the 3D model.

G2 distributions are applied automatically as fraction of the gravity acceleration along *X* and *Y* directions, whereas for G1 distributions, in absence of available load cases in the commercial code, a simplified procedure is utilized, making use of the regular subdivision of the geometrical model and applying loads on two corners of the structure with concentrated forced, as illustrated in Fig. 13. It is worth noting that authors implemented a Matlab user defined subroutine for the automatic evaluation of G1 distributions on a different case study (main tower of the castle and castle), finding very little differences on the final pushover curve, confirming that the simplified procedure here adopted is sufficiently reliable.

Resultant capacity curves of the structure are depicted in Fig. 14 for both G1 and G2 load distributions, for seismic action along *X* and *Y*. Subfigure a refers to the total base shear vs control node horizontal displacement, whereas in subfigure b the acceleration $a_g/g$ vs control node horizontal displacement is represented.

In Fig. 14, collapse loads obtained by means of a FE upper bound limit analysis approach similar to that presented in [24] are also represented. In the model, rigid tetrahedron elements are utilized, with possible plastic dissipation at the triangular interfaces between adjoining elements. The same mesh used for the pushover analyses is adopted, assuming a Mohr–Coulomb failure criterion for the interfaces (with the same mechanical properties of the non-linear static analyses). As can be noted, collapse loads provided by limit analysis fit reasonably well peak loads predicted by pushover simulations, providing an additional confirm of the actual load bearing capacity of the structure.

Deformed shapes at peak (or collapse) provided by the commercial code are reported in Fig. 15. As it is possible to notice, the tower fails for the formation of a flexural–shear hinge near the base of the structure, which appears roughly in agreement to what occurred in reality. The slip surface provided is rather clear and may be isolated manually identifying the elements with maximum plastic dissipation. The difference between behaviors in *X* and *Y* direction is obviously very little, considering the symmetry of the structure and the almost square section of the tower. Results obtained with the pushover analyses are again confirmed by deformed shapes provided by the FE upper bound limit analysis, reported in Fig. 16 for the sake of completeness. It is indeed rather evident in the limit analysis model the formation of a combined flexural–shear hinge in correspondence of the first floor level. Since rigid tetrahedron elements are used in the FE code and plastic dissipation is allowed exclusively at the interfaces, it is experienced a slightly more marked difference between *X* and *Y* directions behavior than that observed in the pushover analyses. In particular, for the seismic load acting along *Y* axis, it is visible the formation of two crack irregular surfaces running along inclined directions, probably a consequence of the presence of small openings in the processing zone. On the contrary, for *X* direction, the cracks seem to develop along a more horizontal direction.

*5.3.1. 1 DOF equivalent system*

On the basis of the 3D non-linear analyses, the seismic vulnerability is evaluated by means of a comparison between the displacement capacity $d_c^*$ and the displacement demand $d_d^*$ obtained by means of the pushover analysis, both referring to the same control point. Control points, in this case, are obviously placed in the middle of one of the edges of the top section and are visualized in Fig. 14. The displacement demand is evaluated with respect to an equivalent single degree-of-freedom system

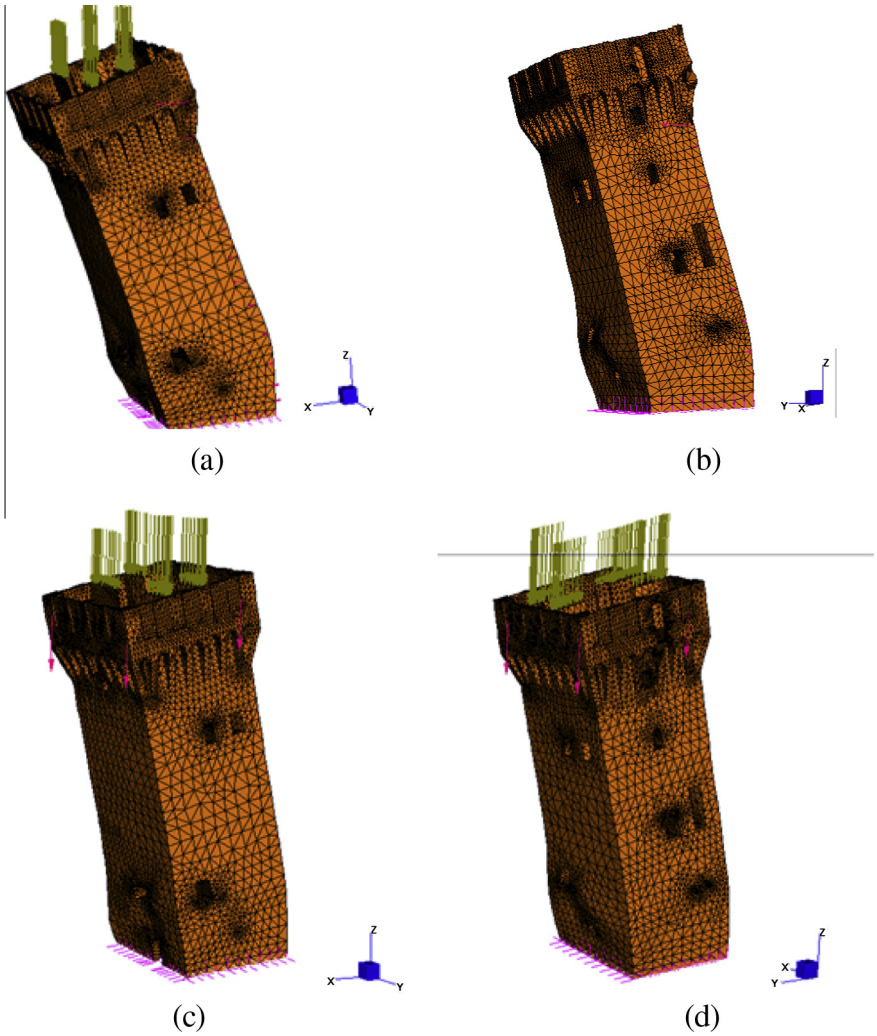


**Fig. 15.** Deformed shapes at peak obtained within the pushover analyses. (a): G1X, (b): G1Y, (c): G2X, (d): G2Y.

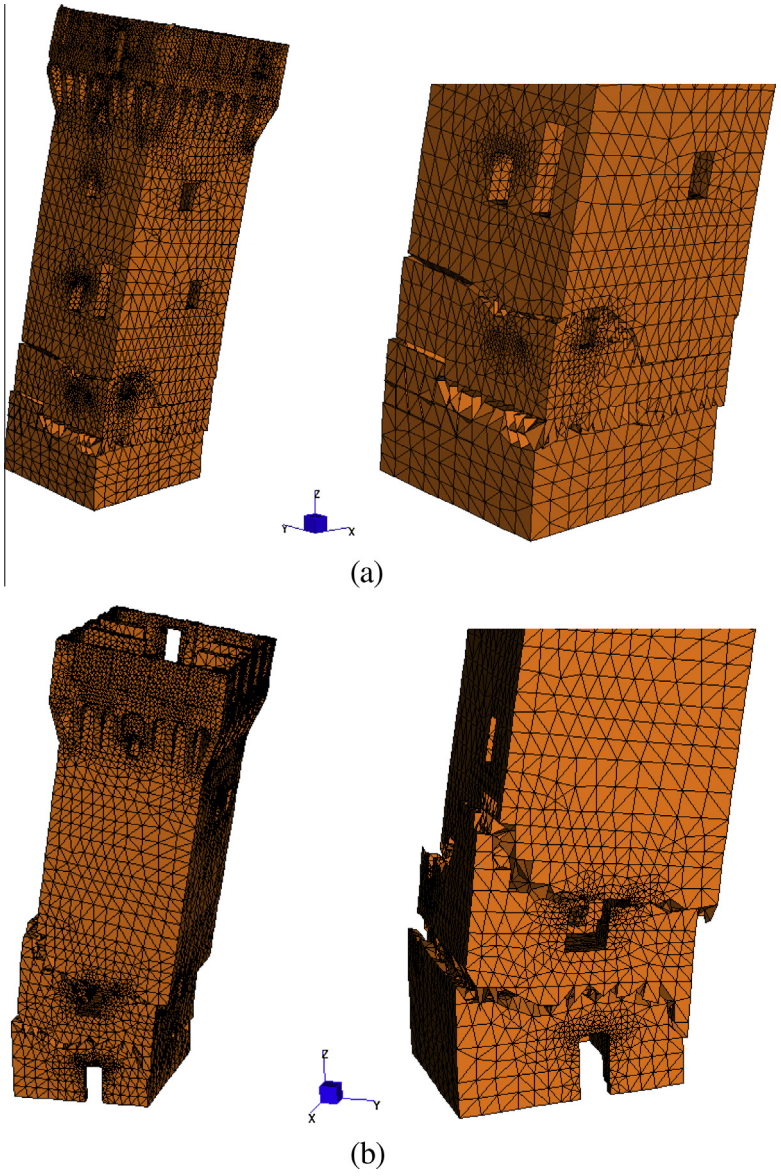


**Fig. 16.** Deformed shapes at failure obtained with the FE upper bound limit analysis (a): G1X, (b): G1Y.

characterized by a bilinear behavior in a shear force–displacement diagram.

As a first step, the pushover curve is scaled by means of the so called participation factor of the fundamental eigenvector $\Gamma = \frac{\sum m_i \Phi_i}{\sum m_i \Phi_i^2}$, where $\Phi_i$ is the $i$th component of the eigenvector $\mathbf{\Phi}$ and $m_i$ is the mass of the node $i$. The fundamental eigenvector $\mathbf{\Phi}$ is deduced from the modal analysis. In particular, in order to evaluate the $\mathbf{\Phi}$ vector, it has been made the reasonable hypothesis that the tower may be approximated with a cantilever beam with concentrated masses on 13 vertical sections, shown in Fig. 9 and normalizing the displacement to the one on the top section. Similarly to the G1 distribution, a Matlab user defined subroutine was implemented in another case study for the exact evaluation of $\mathbf{\Gamma}$, finding negligible differences with the procedure here adopted.

Assuming as $F_b$ and $d_c$ the actual base shear and corresponding displacement of the structure respectively, the scaled values are $F_b^* = F_b/\mathbf{\Gamma}$ and $d_c^* = d_c/\mathbf{\Gamma}$. Assuming as $F_{bu}$ the peak base shear, it follows that $F_{bu}^* = F_{bu}/\mathbf{\Gamma}$.

Once found the pushover curve of the equivalent system ($d_c^*$-$F_b^*$), it is reduced to a bilinear elastic perfectly plastic diagram, whose characteristics, reported in Table 8, are defined as follows. The elastic stiffness $k^*$ is calculated as secant direction of the equivalent capacity curve at a shear force equal to the 70% of the maximum value $F_y^*$. The bilinear diagram is completed assuming an area equivalence between the equivalent and the bi-linear system, where the equivalent curve is stopped at a displacement $d_u^*$ corresponding to a base shear equal to 85% of the peak shear. As usually occurs in complex 3D non-linear analyses, a softening of about 15% is hardly reproducible. The numerical analyses are conducted up to reasonably large displacement, as suggested by the Italian code in

**Table 8**
Characteristic values of the bilinear curves.

| Case | $F^*_y$ (kN) | $a^*_y$ (g) | $k^*$ (kN/mm) | $T^*$ (s) | $d^*_y$ (mm) | $d^*_u$ (mm) | $\mu$ |
|---|---|---|---|---|---|---|---|
| G1X | 705.8 | 0.1636 | 76.2 | 0.47 | 9.3 | 41.6 | 4.50 |
| G1Y | 707.9 | 0.1641 | 83.1 | 0.45 | 8.5 | 41.1 | 4.82 |
| G2X | 995.7 | 0.1238 | 124.0 | 0.37 | 8.0 | 30.5 | 3.79 |
| G2Y | 1020.8 | 0.1242 | 138.5 | 0.35 | 7.4 | 28.1 | 3.82 |

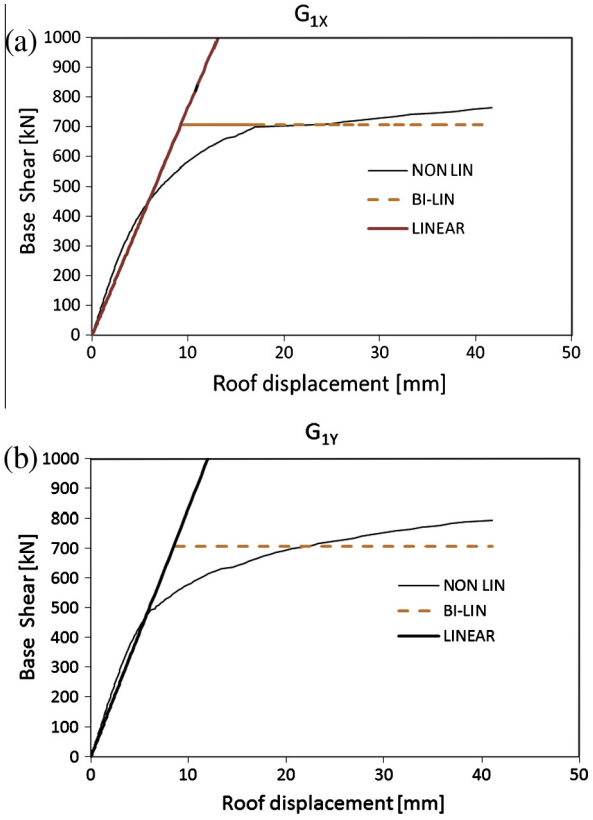


**Fig. 17.** Pushover curves, reduction to a 1DOF elasto-plastic system, G1 distributions.

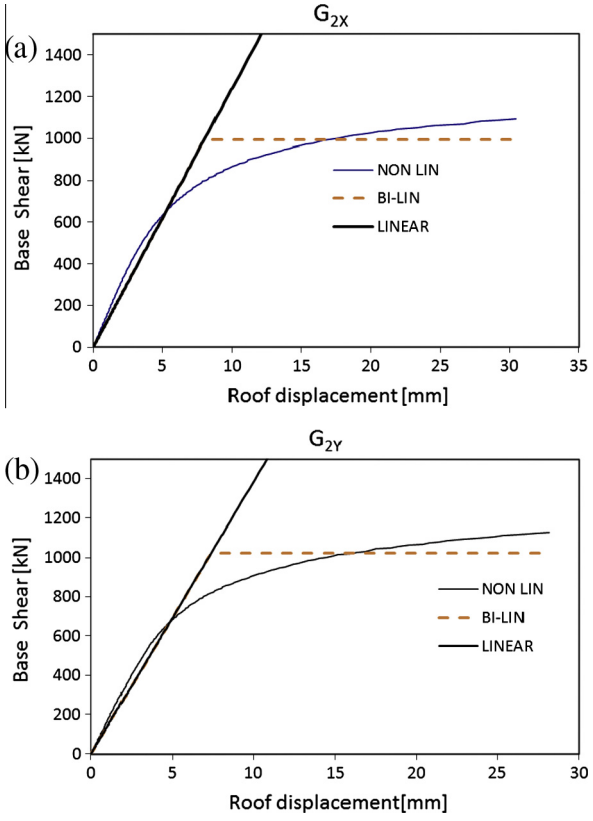


**Fig. 18.** Pushover curves, reduction to a 1DOF elasto-plastic system, G2 distributions.

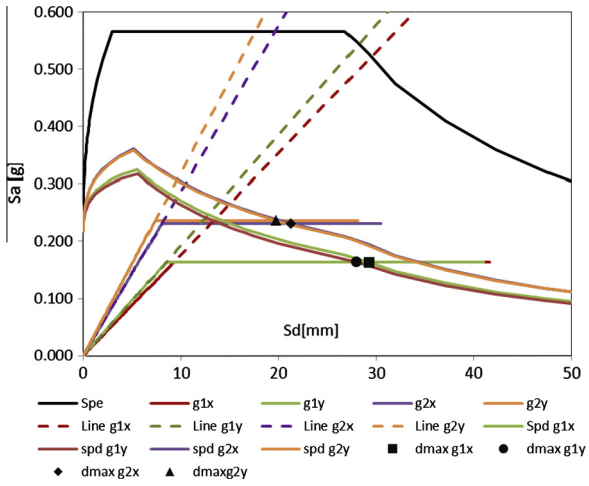


**Fig. 19.** Comparison between displacement capacity and demand, N2 method, class type II and C type soil.

absence of softening materials available, reasonably assumed as collapse state of the structure. The plastic base shear of the 1 DOF equivalent system is called $F_y^*$. In absence of a clear degradation of the base shear, it is assumed $F_y^* = F_{bu}^*$.

The elastic period of the bilinear equivalent system $T^*$ is $T^* = 2\pi\sqrt{m^*/k^*}$ where $m^* = \sum m_i \Phi_i$ = 431,441 kg and $k^* = F_y^*/d_y^*$.

The ductility of the bilinear curve is defined as usual as the ratio between the ultimate and the yield displacement as $\mu = d_u^*/d_y^*$.

Once known $T^*$, the Italian code allows to estimate the displacement demand $d_{\max}^*$ using the elastic displacement spectrum $S_{De}(T)$. The base shear corresponding to $d_{\max}^*$ on the elastic one DOF system is hereafter called $F_e^*$.

Once known $d_{\max}^*$, it has to be checked if $d_{\max}^* \leqslant d_u^*$. For masonry structures, the Italian code requires also that the ratio $q^*$ between the base shear evaluated using the elastic spectrum $F_e^*$ and of the equivalent 1 DOF system $F_y^*$ does not exceed 3.

For the sake of clearness, in Fig. 17 (G1 distribution) and Fig. 18 (G2 distribution), the reduction of the FE pushover curve for the 3D model, seismic directions *X* and *Y*, are represented.

*5.3.2. Assessment by means of the N2 method*

The seismic demands is traditionally defined with a pseudo-accelerations elastic spectrum $S_{ae}(T)$ where the spectral accelerations are defined as a function of the period *T*.

In our case, we will consider the spectra deduced from the Italian code for use class II and both C and D soil type. For each spectrum, it is possible to derive the elastic pseudo-displacement spectrum by means of the following formula:

$$S_{de}(T) = \frac{T^2}{4\pi^2} S_{ae}(T) \tag{8}$$

In order to evaluate the inelastic acceleration–displacement AD spectrum it is necessary (see Fajfar [42]) to use the reduction factor $R_\mu(T)$ linked to the ductility $\mu_s$ and defined as follows:

$$R_\mu(T) = \begin{cases} 1 + (\mu_s - 1)\frac{T}{T_C} & T < T_C \\ \mu_s & T \geqslant T_C \end{cases} \tag{9}$$

where $T_C$ is the end-plateau period of the spectrum and $\mu_s$ is the required ductility.

Conversely $\mu_s$ is dependent on $R_\mu(T^*)$ as follows:

$$\mu_s = \begin{cases} [R_\mu(T^*) - 1]\frac{T_C}{T^*} + 1 & T^* < T_C \\ R_\mu(T^*) & T^* \geqslant T_C \end{cases} \tag{10}$$

**Table 9**
Values derived from the N2 method for a comparison between demand and capacity. Use class II and soil type C. In bold values not verified.

| Case | $a^*_y$ (g) | $T^*$ (s) | $S_{ae}(T^*)$ (g) | $d^*_e$ (mm) | $R_\mu(T^*)$ | $d^*_u$ (mm) | $d^*_{max}$ (mm) | $\mu_R$ | $\mu_S$ |
|---|---|---|---|---|---|---|---|---|---|
| G1X | 0.1636 | 0.47 | 0.527 | 29.27 | **3.22** | 41.6 | 29.27 | 4.50 | 3.22 |
| G1Y | 0.1641 | 0.45 | 0.549 | 27.94 | **3.34** | 41.1 | 27.94 | 4.82 | 3.34 |
| G2X | 0.1238 | 0.37 | 0.566 | 19.31 | 2.45 | 30.5 | 21.36 | 3.79 | 2.71 |
| G2Y | 0.1242 | 0.35 | 0.566 | 17.30 | 2.39 | 28.1 | 19.77 | 3.82 | 2.73 |

**Table 10**
Values derived from the N2 method for a comparison between demand and capacity. Use class II and soil type D. In bold values not verified.

| Caso | $a^*_y$ | $T^*$ (s) | $S_{ae}(T^*)$ (g) | $d^*_e$ (mm) | $R_\mu(T^*)$ | $d^*_u$ (mm) | $d^*_{max}$ (mm) | $\mu_R$ | $\mu_S$ |
|---|---|---|---|---|---|---|---|---|---|
| G1X | 0.1636 | 0.47 | 0.693 | 38.52 | **4.24** | 41.6 | 49.53 | 4.50 | 5.45 |
| G1Y | 0.1641 | 0.45 | 0.693 | 35.31 | **4.23** | 41.1 | 47.05 | 4.82 | 5.63 |
| G2X | 0.1238 | 0.37 | 0.693 | 23.66 | **3.00** | 30.5 | 35.55 | 3.79 | 4.52 |
| G2Y | 0.1242 | 0.35 | 0.693 | 21.20 | 2.93 | 28.1 | 33.10 | 3.82 | 4.58 |

**Table 11**
Comparison between displacement demand and capacity and ductility, D soil type.

| $d^*_u$ (mm) | $d^*_{max}$ (mm) | $\Delta d$ (%) | $\mu_R$ | $\mu_S$ | $\Delta\mu$ (%) |
|---|---|---|---|---|---|
| 41.6 | 49.53 | 19.0 | 4.50 | 5.45 | 21.3 |
| 41.1 | 47.05 | 14.5 | 4.82 | 5.63 | 16.7 |
| 30.5 | 35.55 | 16.7 | 3.79 | 4.52 | 19.0 |
| 28.1 | 33.10 | 17.6 | 3.82 | 4.58 | 19.9 |

where $R_\mu(T^*) = S_{ae}(T^*)/a^*_y$, with $S_{ae}(T^*)$ acceleration found with the elastic acceleration spectrum in correspondence of the period of the equivalent 1 DOF system and $a^*_y$ the plasticization acceleration.

The inelastic acceleration spectrum is defined as the ratio between the elastic spectrum and the reduction factor as $S_a(T) = S_{ae}(T)/R_\mu(T)$.

The inelastic spectrum of the pseudo displacements is evaluated as $S_d(T) = S_{de}(T)\mu_s/R_\mu(T)$.

Finally, to find the displacement demand, it can be used either the graphical procedure (intersection of the bilinear equivalent system with $S_d(T)$) or the following analytical relationship:

$$d^*_{max} = \begin{cases} \left[1 + (R_\mu(T^*) - 1)\frac{T_C}{T^*}\right]\frac{d^*_e}{R_\mu(T^*)} & T^* < T_C \\ S_{de}(T^*) & T^* \geqslant T_C \end{cases} \quad (11)$$

where $d^*_e = S_{de}(T^*)$.

In Fig. 19 the graphical representation in the AD plane of the N2 method for the pushover analyses conducted is reported. The hypothesis of soil C is made. Four cases are represented, assuming G1 and G2 loads distributions and the two orthogonal directions X–Y.

Points corresponding to $d^*_{max}$ are also depicted. If $d^*_{max}$ belongs to the capacity curve (i.e. $d^*_{max} < d^*_u$) and if a further condition according to the Italian code holds, i.e. $R_\mu(T^*) < 3$, then the structure is verified. A synopsis of the results obtained is represented in Tables 9 and 10.

From an overall analysis of the results, it can be observed that only for G2 load distribution the intersection between the line of the elastic part of the bilinear curve and the elastic displacement-acceleration spectrum falls within the extremes of the plateau of the spectrum. For G1 load distribution, the intersection occurs in the descending branch, meaning that the period of the elastic 1DOF system is lower than $T_C$ for G2 and greater than $T_C$ for G1. Such intersection points represent the acceleration $S_{ae}(T^*)$ and the displacement $d_e{}^*$ associated to a system with a purely elastic behavior.

The acceleration $a^*_y$, identified by the $y$-values of the horizontal line in the bilinear system for G1X, G1Y, G2X e G2Y, represents both the capacity acceleration and that imposed by the load distribution to an inelastic system.

The intersection of such horizontal lines with the displacement spectrum identifies the demand in terms of displacement. Conversely, if the bilinear system does not intersect the displacement spectrum, it means that the structure is not able to safely withstand the horizontal loads distribution. Note that $d_e{}^*$ is equal to $d^*_{max}$ for G1X configuration, being $T^* > T_C$.

From the N2 analyses, it can be stated that the structure has the resources to reach the seismic induced displacement when considering a use class II and a C soil type. Values reported in Table 11 confirm that the ultimate displacements and the ductility of the capacity curve are greater than those imposed by loads distributions. However, for G1 distributions along both directions the ratio $R_\mu(T^*)$ is greater than 3. The seismic assessment, therefore, should be considered not passed.

The same procedure is repeated for use class II and soil D and the results are summarized in Fig. 20. As can be noted, again G1 bilinear curves are critical and the demand results greater than the capacity (no intersection). The tower results therefore unsafe under the hypotheses done.

In Table 11, a synopsis of the displacement (demand and capacity) and ductility values required is reported to have a general insight into the behavior of the tower under the different load conditions and hypotheses done, especially on the soil type. As can be noted, the structure is generally unsafe, meaning that Code of Practice spectrum, which for Finale Emilia well approximates the actual one occurred during the seismic event for long return period, see Fig. 7, corresponds to an unsafe state for the structure.

### 5.4. Dynamic analyses

In order to capture all possible failure mechanisms, the effect of the earthquake should be considered by a non-linear dynamic analysis, namely, by applying at the base of the building an acceleration history whose shape and intensity can be defined upon a natural registration or artificially generated. Such kind of analysis is very time consuming; however, it is much more accurate and reliable than other approaches for its capability to evidence in plane and out of plane, as well as local and global failure mechanisms.

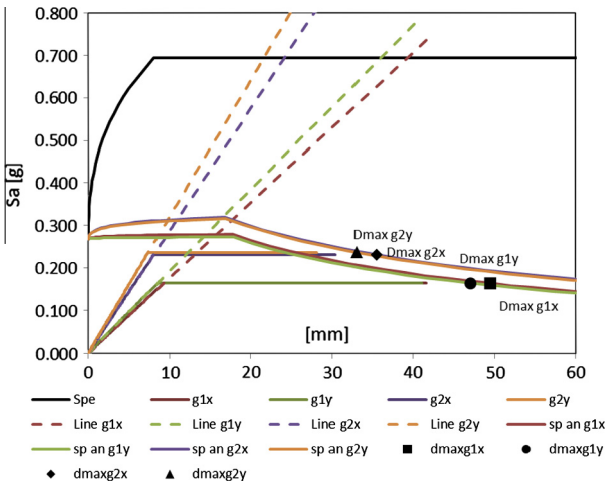


**Fig. 20.** Comparison between displacement capacity and demand, N2 method, class type II and D type soil.

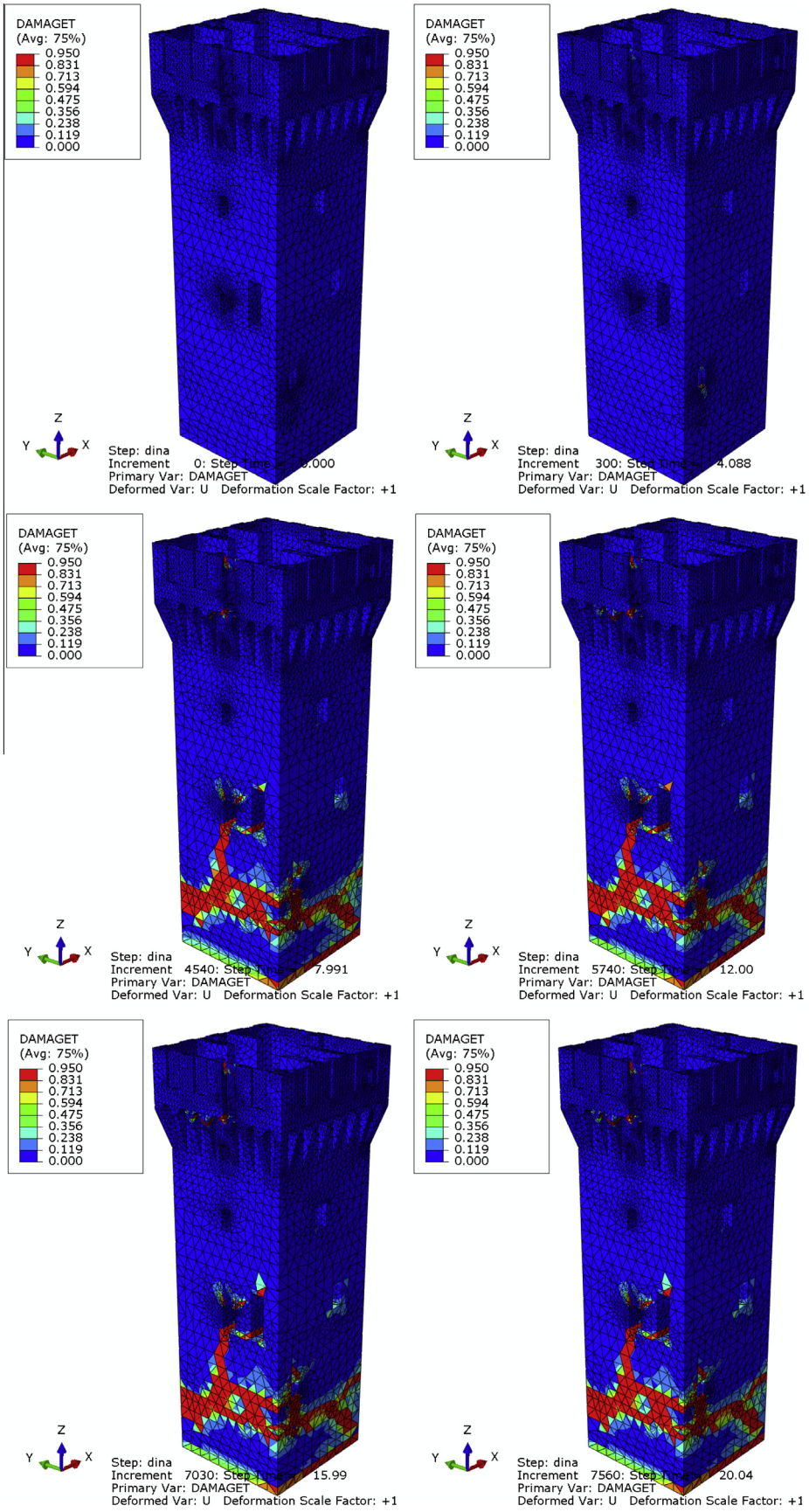


**Fig. 21.** South-west view. Deformed configuration and tensile damage distribution. Frames are returned at the instants 0.0 s, 4.0 s, 8.0 s, 12 s, 16 s, 20 s. Scaling factor = 1 x.

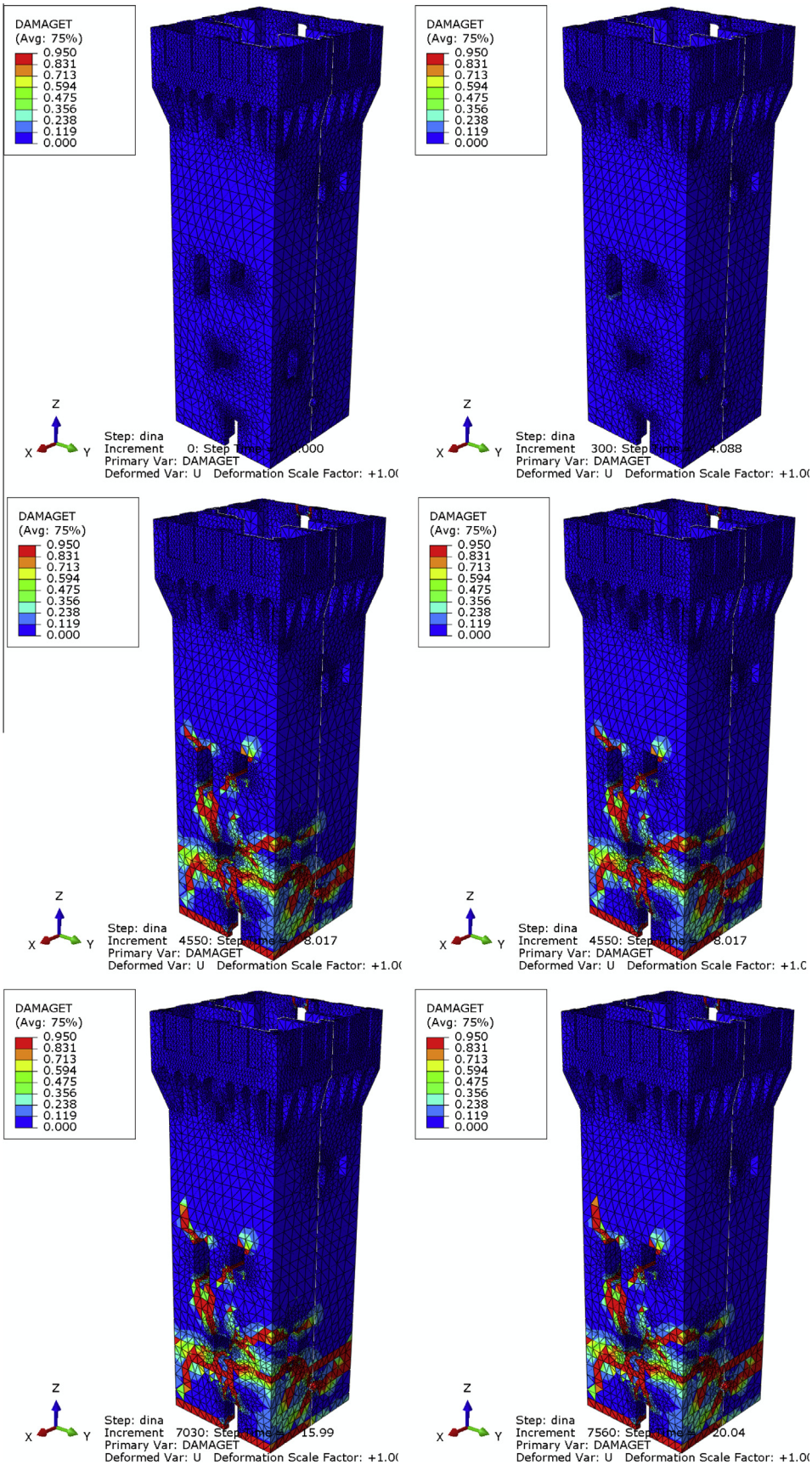


**Fig. 22.** North-east view. Deformed configuration and tensile damage distribution. Frames are returned at the instants 0.0 s, 4.0 s, 8.0 s, 12 s, 16 s, 20 s. Scaling factor = 1 x.

Based on these information, the three-dimensional finite element model of the entire structure is implemented in ABAQUS [26], taking into consideration geometrical (large displacement effects) and material nonlinearity (elasto-plastic with damaging behavior of the masonry material), with the aim of investigating the seismic behavior of the structure by means of a non-linear dynamic analysis.

As already pointed out, a step-by-step non-linear dynamic analysis is definitely the most appropriate non-standard numerical procedure to evaluate the actual behavior of masonry structures during earthquakes. However, at present, adequate commercial numerical codes are not easily available and the analysis itself requires experienced users, especially with regard to the constitutive aspects (the post-elastic, hysteretic behavior of the structure, and the consequent energy dissipation, should be consistently reproduced). The choice of significant input accelerograms is still a controversial question. When speaking of historical and monumental buildings, the question is even more critical: nearly all the structural analysis methods suffer from a lot of uncertainties and limitations, mainly derived from the incompleteness of the knowledge level, from the presence of widespread inhomogeneities and nonlinearities and a complex constructive history.

The 3D geometrical model of the tower was imported into ABAQUS [26], and as a compromise between the conflicting requirements of reasonable computing time and accuracy of the solution a finite element discretization, based on four nodes tetrahedral elements, having an average size of 0.40 m was adopted. The total number of elements is equal to 136804 for a total number of 97,152 degrees of freedom. In particular the mesh was refined near the openings, where the main failure mechanisms are likely to start. Since not negligible out of plane displacement may occur during a seismic event, large displacement effects are considered. Perfect connection is assumed between perpendicular walls.

Despite the general drawbacks and aforementioned limitations regarding the dynamic analyses, the use of sophisticated 3D models requires a relatively reasonable computational effort, if the discretizations are not excessively refined and the material models does not exhibit strong softening.

The full dynamic analyses were performed by using the real accelerogram registered not far from the tower during the first seismic shake (20th May). Here it is worth noting that in the model both the vertical and horizontal accelerograms have been applied for the dynamic analyses. A vertical ground motion, indeed, could be potentially rather important, especially for slender structures and when the structure is located near the epicenter of the earthquake.

In Fig. 6 the input accelerograms used are shown. In Figs. 21–23, the tensile damage patch is shown at successive time steps and from different points of view.

From an overall analysis of simulations results, it is possible to notice that the tower exhibits significant damage for the earthquake excitation occurred. Some elements undergo very large displacements. Comparing the crack patterns at the end of the simulations, it appears rather clear that the tower collapses for

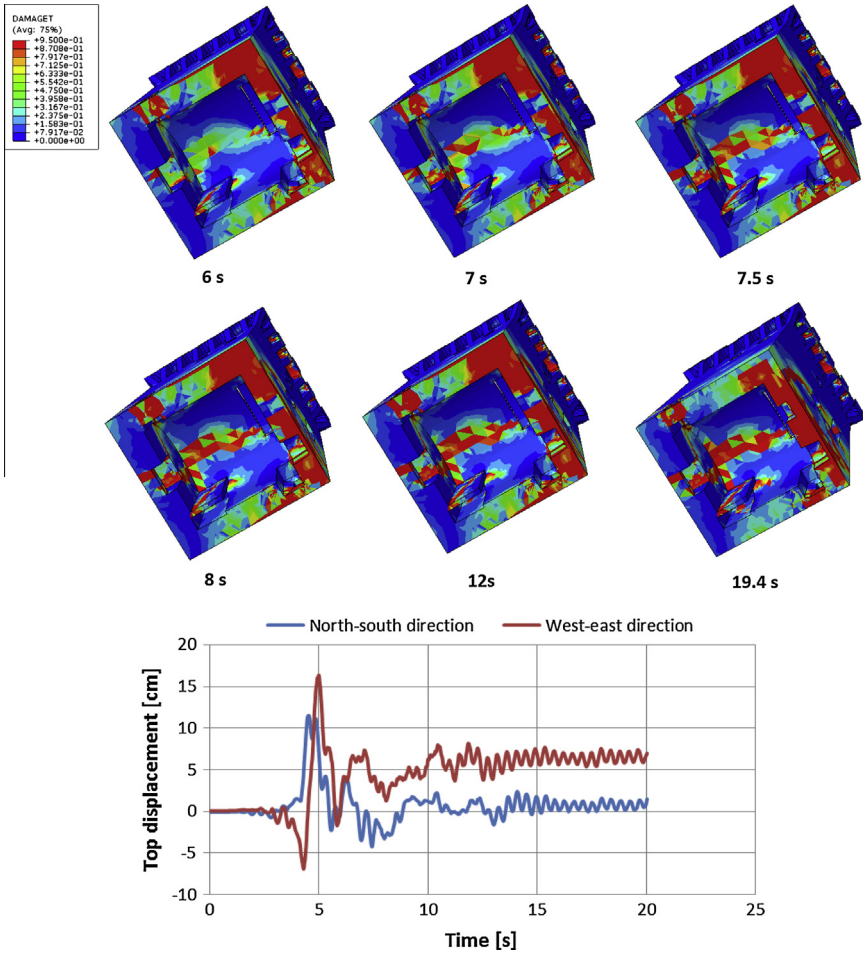


**Fig. 23.** Top and center: damage evolution from 6 to 19.4 s. Detail of the first floor cylindrical vault. Bottom: Displacement along both north–south and west–east directions, measured at the top of the tower.

the formation of a shear-flexural hinge in the lower region of the tower, immediately over the ground floor vault, as evidenced by the inclined path of the formed crack. While some evident differences between present deformed shapes and non-linear static ones may be remarked, the dynamic behavior of the tower has some similarities with that occurred in reality, such as the formation of a mixed shear and flexural hinge near the first floor level. This is not surprising, since it is largely demonstrated that static incremental analyses following a first mode deformation scheme may not reproduce realistically the failure mechanism induced by a dynamic analysis, which, on the contrary, is also able to take into account the contribution of the higher modes, which may become very important to reproduce the effective collapse mechanism occurred in the reality.

In Figs. 21 and 22, it is particularly evident how the damage spreads very quickly on the base section with a concentration almost exclusively on the West corner, which is subjected to severe traction stresses. On the Nord side, damage spreads on the region between the upper part of the ground floor and lower part of the first floor. On the East side, where the main entrance to the tower was located, the analysis predicts a tensile damage spreading in the vertical direction, similar to the crack occurred in reality during the earthquake, which caused the collapse of the structure.

Fig. 23 visualizes also the displacement along both north–south and west–east directions, measured at the top of the tower as a function of time. A maximum top displacement as large as 16 cm was computed after about 5 s from the beginning of the earthquake, instant at which, as evidenced by Figs. 21 and 22, the main non-linear phenomena occurred. At the end of the seismic excitation a residual displacement of 5 cm along the west–east direction emphasizes once more that these are the sides of the tower that much suffered.

## 6. Conclusions

The standard and non-standard numerical analyses conducted on the clock tower all agree in highlighting the very low resistance of the tower against horizontal actions and its intrinsic vulnerability.

They also give a comprehensive answer to the basic question on the reason why the tower collapsed. All the indicators, indeed, agree in evaluating the structure as unsafe under both the code of practice seismic action and that actually occurred during the seismic event.

The reason at the base of the tower high vulnerability is mainly linked to the very poor mechanical properties of the constituent materials, especially when dealing with the mortar joints.

Visual inspection on triplets of ruined walls, indeed, showed almost zero cohesion for the joints, with a visible degradation of the mortar.

Possible guidelines for the reconstruction should consider, in the authors' opinion, a consistent upgrading of the mortar mechanical properties, eventually by means of special products, as well as the strengthening of the survived lower part and of the foundation, by means of mortar injection and improved interlocking between internal and external leaves.

## Acknowledgements

Arch. Carla Di Francesco, responsible for the Emilia Romagna region of the Italian Ministry of the Architectural Heritage (MiBAC) is gratefully acknowledged for making possible the cooperation between Technical University of Milan and MiBAC.

Mr. Fernando Ferioli, mayor of Finale Emilia town, is gratefully acknowledged for making possible the cooperation between Technical University of Milan and Finale Emilia municipal administration.

Mr. Massimo Righini, culture council member of Finale Emilia town, is gratefully acknowledged for the constant passion in providing architectural and historical information on the tower.

## References

[1] Milani G, Acito M, Bocciarelli M, Chesi C. Advanced numerical analyses on two historical masonry structures in Finale Emilia (Italy) severely damaged by the May 2012 Emilia Romagna seismic event. In: Altay Gülay, Mazzolani Federico, editors. Proc. 2nd international conference of protection of historical constructions PROHITECH 2014, Antalya, Turkey, 7–9 May 2014.
[2] Acito M, Milani G, Chesi C, Vallè M, Sumini V. Collapse of the clock-tower in Finale Emilia after the Emilia-Romagna seismic events in May 2012: a numerical insight. In: Proc. XV Convegno ANIDIS. L'ingegneria sismica in Italia, Padova; June 30th–July 4th, 2013.
[3] Binda L, Zanzi L, Lualdi M, Condoleo P. The use of georadar to assess damage to a masonry bell tower in Cremona, Italy. NDT&E Int 2005;38:171–9.
[4] Lourenço PB. Assessment, diagnosis and strengthening of Outeiro Church, Portugal. Constr Build Mater 2005;19:634–45.
[5] Modena C, Valluzzi MR, Tongini FR, Binda L. Design choices and intervention techniques for repairing and strengthening of the Monza cathedral bell-tower. Constr Build Mater 2002;16:385–95.
[6] Anzani A, Binda L, Carpinteri A, Invernizzi S, Lacidogna G. A multilevel approach for the damage assessment of historic masonry towers. J Cult Heritage 2010;11:459–70.
[7] Carpinteri A, Invernizzi S, Lacidogna G. In situ damage assessment and nonlinear modelling of a historical masonry tower. Eng Struct 2005;27(3):387–95.
[8] Ivorra S, Pallares FJ. Dynamic investigations on a masonry bell tower. Eng Struct 2006;28:660–7.
[9] Russo G, Bergamo O, Damiani L, Lugato D. Experimental analysis of the "Saint Andrea" Masonry Bell Tower in Venice. A new method for the determination of "Tower Global Young's Modulus E". Eng Struct 2010;32:353–60.
[10] Abruzzese D, Miccoli L, Yuan J. Mechanical behavior of leaning masonry Huzhu Pagoda. J Cult Heritage 2009;10:480–6.
[11] Riva P, Perotti F, Guidoboni E, Boschi E. Seismic analysis of the Asinelli Tower and earthquakes in Bologna. Soil Dynam Earthq Eng 1998;17:525–50.
[12] Bernardeschi K, Padovani C, Pasquinelli G. Numerical modelling of the structural behaviour of Buti's bell tower. J. Cultural Heritage 2004;5:371–8.
[13] Bayraktar A, Sahin A, Özcan M, Yildirim F. Numerical damage assessment of Haghia Sophia bell tower by nonlinear FE modeling. Appl Math Model 2010;34:92–121.
[14] Milani G, Russo S, Pizzolato M, Tralli A. Seismic behavior of the San Pietro di Coppito church bell tower in L'Aquila, Italy. Open Civ Eng J 2012;6(Sp. Issue #1):131–47.
[15] Carpinteri A, Invernizzi S, Lacidogna G. Numerical assessment of three medieval masonry towers subjected to different loading conditions. Masonry Int 2006;19:65–75.
[16] Casolo S, Milani G, Uva G, Alessandri C. Comparative seismic vulnerability analysis on ten masonry towers in the coastal Po Valley in Italy. Eng Struct 2013;49:465–90.
[17] Pena F, Lourenço PB, Mendez N, Oliveira D. Numerical models for the seismic assessment of an old masonry tower. Eng Struct 2010;32:1466–78.
[18] Milani G, Casolo S, Naliato A, Tralli A. Seismic assessment of a medieval masonry tower in Northern Italy by limit, non-linear static and full dynamic analyses. Int J Archit Heritage 2012;6(5):489–524.
[19] NTC 2008. Nuove norme tecniche per le costruzioni. Ministero delle Infrastrutture (GU n.29 04/02/2008), Rome, Italy; 14/01/2008.
[20] OPCM 3274 2003. Ordinanza del Presidente del Consiglio dei Ministri n.3274 20/03/2003: Elementi in materia di criteri generali per la classificazione sismica del territorio nazionale e di normative tecniche per le costruzioni in zona sismica e successivi aggiornamenti.
[21] OPCM 3431 2005. Ordinanza del Presidente del Consiglio dei Ministri n.3431 09/05/2005. Ulteriori modifiche ed integrazioni all'OPCM 3274/03 [in Italian].
[22] Circolare 2009. Circolare n. 617 del 2 febbraio 2009 Istruzioni per l'Applicazione Nuove Norme Tecniche Costruzioni di cui al Decreto Ministeriale 14 gennaio 2008.
[23] Linee guida per la valutazione e la riduzione del rischio sismico del patrimonio culturale, Ministero per i beni e le attività culturali MiBAC, Italy; 2011.
[24] Milani G. 3D upper bound limit analysis of multi-leaf masonry walls. Int J Mech Sci 2008;50(4):817–36.
[25] STRAUS7®. Theoretical manual-theoretical background to the Strand7 finite element analysis system; 2004.
[26] ABAQUS®. Theory manual, version 6.6; 2006.
[27] Bignami C et al. Coseismic deformation pattern of the Emilia 2012 seismic sequence imaged by Radarsat-1 interferometry. Ann Geophys 2012;55:4.
[28] Iervolino I, Chioccarelli E, De Luca F. Preliminary study of Emilia (May 20th 2012) earthquake ground motion records. Reluis report V2.11; 2012. <http://www.reluis.it>.
[29] Iervolino I, Chioccarelli E, De Luca F. Engineering seismic demand in the 2012 Emilia sequence: Prelimi-nary analysis and model compatibility assessment. Ann Geophys 2012:55.

[30] Petti L, Lodato A. Preliminary spatial analysis and comparison between response spectra evaluated for Emilia Romagna earthquakes and elastic demand spectra according to the new seismic Italian Code. Reluis report; 2012. <http://www.reluis.it>.
[31] Milani G. Lesson learned after the Emilia Romagna, Italy, 20–29 May 2012 earthquakes: a limit analysis insight on three masonry churches. Eng Fail Anal 2013;34:761–78.
[32] Barbieri G, Biolzi L, Bocciarelli M, Fregonese L, Frigeri A. Assessing the seismic vulnerability of a historical building. Eng Struct 2013;57:523–35.
[33] Artioli M, Battaglia R, Tralli A. Effects of May 2012 Emilia earthquake on industrial buildings of early '900 on the Po river line. Eng Struct 2013;56: 1220–33.
[34] Lourenço PB, Rots J. A multi-surface interface model for the analysis of masonry structures. J Eng Mech ASCE 1997;123(7):660–8.
[35] Milani G, Lourenço PB, Tralli A. Homogenised limit analysis of masonry walls. Part I: failure surfaces. Comput Struct 2006;84:166–80.
[36] Milani E, Milani G, Tralli A. Limit analysis of masonry vaults by means of curved shell finite elements and homogenization. Int J Solids Struct 2008;45:5258–88.
[37] Luciano R, Sacco E. Damage of masonry panels reinforced by FRP sheets. Int J Solids Struct 1998;35(15):1723–41.
[38] Lourenço PB, de Borst R, Rots J. A plane stress softening plasticity model for orthotropic materials. Int J Numer Meth Eng 1997;40:4033–57.
[39] Van Der Pluijm. Shear Behaviour of bed joints. In: Abrams DP, editor. Proceedings of 6th North American masonry conference, Philadelphia; 6–9 June, 1993. p. 125–36.
[40] Page A. The biaxial compressive strength of brick masonry. Proc Inst Civil Eng. 1981;71:893–906.
[41] Alessandri C, Di Francesco C, Guerzoni G. L'Abbazia di Pomposa: analisi di un dissesto e proposta di consolidamento. Costruire Laterizio 2000;74:48–53.
[42] Fajfar P. A nonlinear analysis method for performance-based seismic design. Earthq Spectra 2000;16(3):573–92.